communications biology

A Nature Portfolio journal

Article

https://doi.org/10.1038/s42003-025-08656-x

HEP14-activated PKC-ERK1/2 pathway boosts HEP14-empowered hADSCs for ovarian regeneration and functional restoration

Jiajia Sun[1,2,8], Qin Zhong[3,8], Kan Liu[1,2], Qili Sun[4], Chunan Lu[4], Yingtong Di[5], Lin Bai[6], Helen Picton[7], Bin Tang[4] ✉, Xiaojiang Hao[5] ✉ & Liming Gui[1,2,3] ✉

Premature ovarian insufficiency (POI) and age-related natural-aging ovarian insufficiency (ARNA-OI) pose pressing global health challenges, necessitating effective therapeutic strategies and a deep understanding of their underlying mechanisms. This study investigates how HEP14, a PKC pathway activator, boosts the regenerative potential of human adipose-derived stem cells (hADSCs) for ovarian regeneration. Transcriptome analysis reveals that HEP14 modulates gene expression profile in hADSCs, enhancing their regenerative capacity. In mouse models of POI and ARNA-OI, co-administration of HEP14-empowered hADSCs (h-hADSCs) with HEP14/PLGA microspheres significantly improves ovarian regeneration and function. These effects are attributed to increased h-hADSC retention and transdifferentiation, enhanced antifibrotic and proangiogenic capability, along with an optimized dosing strategy. The upregulation of MMP1, PDGFD, and STC1 through the HEP14-activated PKC-ERK1/2 signaling pathway is crucial for these effects. Our findings highlight the pivotal role of h-hADSCs and the HEP14-activated PKC-ERK1/2 pathway in ovarian regeneration and provide a promising advancement in treating ovarian insufficiency.

Ovarian insufficiency (OI) is caused by a reduction or depletion of the follicular pool and stromal fibrosis within the ovaries, leading to diminished ovarian function and associated complications[1,2]. This includes premature ovarian insufficiency (POI) and age-related natural-aging ovarian insufficiency (ARNA-OI). POI frequently arises as a significant complication of anticancer therapies and results in infertility, affecting approximately 1–6% of women under the age of 40[3,4]. ARNA-OI, on the other hand, represents the natural aging process of the female reproductive system, which typically declines a decade earlier than other organs in women and affects multiple systems of the body[2,5]. Current therapeutic interventions demonstrate limited efficacy and/or carry potential risks[6,7]. As a results, the quest for efficacious treatments for OI and an understanding of their underlying mechanisms has become a focal point of research.

Mesenchymal stem cells (MSCs)-based therapies have shown promising prospects in regenerative medicine. However, this field still faces numerous challenges, primarily stemming from an incomplete understanding of MSCs' therapeutic mechanisms, compounded by issues such as low stem cell survival rates, inconsistent differentiation, cellular senescence, limited tissue receptivity, and the need to optimize administration routes[8,9]. To tackle these impediments, research has increasingly focused on developing tissue-targeted therapies and elucidating their therapeutic mechanisms, aiming to create highly efficient treatment systems utilizing MSCs. Various methods have been reported to enhance the therapeutic efficacy of MSCs through genetic engineering, chemical modification, pretreatment, and magnetic targeting in the context of other diseases. Nevertheless, these approaches exhibit notable limitations and challenges[8–10]. It is noteworthy

[1]Institute of Obstetrics and Gynecology, Shenzhen Peking University-Hong Kong University of Science and Technology Medical Center Medical Center, Shenzhen, China. [2]Department of Obstetrics and Gynaecology, Peking University Shenzhen Hospital, Shenzhen, China. [3]Centre for Tissue Engineering and Stem Cell Research, Guizhou Medical University, Guiyang, China. [4]Department of Biomedical Engineering, Southern University of Science and Technology, Shenzhen, China. [5]State Key Laboratory of Phytochemistry and Plant Resource in West China, Kunming Institute of Botany, Chinese Academy of Sciences, Kunming, China. [6]Institute of Laboratory Animals Science, Chinese Academy of Medical Sciences, Beijing, China. [7]Reproduction and Early Development Research Group, Discovery and Translational Science Department, Leeds Institute of Cardiovascular and Metabolic Medicine, School of Medicine, University of Leeds, Leeds, UK. [8]These authors contributed equally: Jiajia Sun, Qin Zhong. ✉e-mail: tangb@sustech.edu.cn; haoxj@mail.kib.ac.cn; dawnkwei@163.com

that there is a considerable lack of pertinent research focused on enhancing the therapeutic efficacy of MSCs and thoroughly elucidating their underlying mechanisms responsible for their potential in addressing OI. Currently, there is no Food and Drug Administration (FDA)-approved stem cell therapy specifically tailored for OI. Therefore, continued attention to both basic research and clinical trials is imperative to propel the field of OI treatment forward.

HEP14 is a natural small molecule and novel activator of Protein Kinase C (PKC) pathway[11]. Activation of PKC and its downstream signaling molecules such as extracellular regulated protein kinases 1/2 (ERK1/2) are implicated in the regulation of a wide variety of cellular processes, including cell growth, differentiation, and survival/apoptosis[12]. Nowadays, the concept of precision medicine has taken firm root. Human adipose-derived stem cells (hADSCs), isolated from fat tissue, currently represents a more practical source of MSCs compared to other source[13]. Our preliminary experiments suggested that HEP14 treatment enhanced hADSC viability and stemness in primary culture, and these cells were designated as HEP14-empowered hADSCs (h-hADSCs). Bulk RNA-sequencing analysis uncovered that the differentially expressed genes (DEGs) enriched in the biological processes, including extracellular matrix (ECM) remodeling, angiogenesis, cell fate commitment, ovarian steroidogenesis, and the activation of MAPK activity in h-hADSCs. These processes may be strongly involved in ovarian tissue remodeling and regeneration. Furthermore, single-cell RNA-sequencing analysis revealed that h-hADSCs highly expressed key genes characteristic of ovarian granulosa cells (GCs) and theca cells (TCs), as previously reported[14]. This suggests that HEP14 may predispose hADSCs to transdifferentiate into ovarian cell-like cells. The regulation of PKC pathway is a recognized method of physiologically changing cells[15], however, its application in the context of stem cell therapy remains underexplored. In this study, we investigate the therapeutic efficacy of h-hADSCs alone or in combination with HEP14 loaded Poly (lactic-co-glycolic acid) (PLGA) microspheres (HEP14/PLGA microspheres) and underlying action mechanisms by using mouse models of chemotherapy drug doxorubicin-induced POI and ARNA-OI. PLGA particles, FDA-approved and known for excellent drug loading and safety, are ideal carriers for achieving therapeutic goals and enhancing clinical success[16,17]. As shown in our previous work[18], PLGA was utilized as a drug carrier to fabricate HEP14/PLGA microspheres for ensuring a sustained release of HEP14 for in vivo applications.

Stem cell-based therapy relies critically on the quantity of transplanted stem cells and their ability to differentiate into functional cells and to secrete vital growth factors[19]. A delicate interplay of autocrine, endocrine, and paracrine pathways regulate folliculogenesis and ovarian regeneration, stressing the importance of direct interaction among follicles, transplanted stem cells, and altered secretome components for effective tissue regeneration and functional restoration[20]. We therefore administered h-hADSCs via intraovarian (i.o.) injection either alone or in combination with HEP14/PLGA microspheres via intraperitoneal (i.p.) injection in mice with OI. These selected delivery routes for h-hADSCs and HEP14/PLGA microspheres were specifically designed to circumvent the constraints of ovarian receptivity and to ensure a sustained release of HEP14 from the HEP14/PLGA microspheres in vivo, thereby augmenting the therapeutic efficacy of the transplanted h-hADSCs. This strategy led to a marked improvement in ovarian remodeling by HEP14-activated PKC-ERK1/2-MMP1, -PDGFD, and -STC1 pathways in model mice with either POI or ARNA-OI. The therapeutic approaches developed based on these findings are set to make significant contributions to the field of reproductive and regenerative medicine.

Results

HEP14 enhanced the viability and stemness of human adipose-derived stem cells

hADSCs, isolated using a modified, previously established method[21], exhibited a fibroblast-like morphology (Fig. S1A). Flow cytometry confirmed their identity, with >96% expressing CD73, CD90, CD105 and CD29, while being negative for CD31 or HLA-DR (Fig. 1A). Their osteogenic and adipogenic potential was verified by Alizarin red and oil red staining (Fig. S1B and C). HEP14's chemical structure is shown in Fig. S1D. CCK8 assays revealed that HEP14 treatment enhanced the viability and proliferation of hADSCs in a dose- and time-dependent manner compared to vehicle-treated hADSCs as control. Among the tested concentrations, a HEP14 concentration of 2.5 μM was identified to be the most effective in promoting hADSC viability and proliferation (Fig. 1B and C). This optimal concentration was therefore selected for subsequent experiments. Flow cytometry showed an increased S phase and decreased G2/M phase in HEP14-treated hADSCs (Fig. S1E and F). Growth kinetics analysis indicated a shorter population doubling time for HEP14-treated hADSCs (19.2 h) and vehicle-treated hADSCs (21.1 h) (Fig. 1D). Real-time qPCR, western blot, and immunofluorescence (IF) staining confirmed upregulated expression of pluripotency marker NANOG and mesenchymal stem cell proliferative marker NUCLEOSTEMIN in HEP14-treated hADSCs (Fig. 1E–G). These findings suggest that HEP14 enhances the viability and stemness of hADSCs. Hereafter, hADSCs treated with HEP14 are referred to as h-hADSCs, while those treated with vehicle are termed as c-hADSCs.

HEP14 changed the transcriptomic profile of hADSCs

To gain insight into the action mechanism of HEP14 on h-hADSCs, bulk and single-cell RNA-sequencing were performed on h-hADSCs and c-hADSCs. HEP14 altered the transcriptomic profile of h-hADSCs. Bulk RNA-seq (GSE273949) identified 1003 DEGs in h-hADSCs vs c-hADSCs, with 573 upregulated genes and 430 downregulated genes (Fig. 2A and B), implicated in ECM organization, angiogenesis, tissue remodeling, cell fate, ERK1 and 2 cascade, positive regulation of MAPK cascade and steroid metabolic process in the biological processes (Fig. 2C). A sub-heatmap of the key DEGs was reconstructed in the h-hADSCs that are closely associated with tissue remodel and regeneration (Fig. 2D). Real-time qPCR validated the expression of key genes, as shown in Fig. 2E and F. In support, gene set enrichment analysis (GSEA) correlated HEP14-regulated genes with ECM-receptor interaction, cell fate, blood vessel formation, ovarian steroidogenesis, and MAPK activity (Fig. 2G–K). scRNA-seq revealed 14 clusters in h-hADSCs vs 9 clusters in c-hADSCs (GSE273950), indicating diverse cell fate transitions (Fig. S2A). Analysis of representative marker genes at single-cell level indicated that h-hADSCs showed high expression of representative key genes for ovarian granulosa cells, theca cells, and tissue remodeling compared with c-hADSCs (Fig. 2L). These results were validated through uniform manifold approximation and projection analysis (Fig. S2B). These findings support the potential role of HEP14 in enhancing the effects of h-hADSCs on ovarian regeneration and functional restoration.

h-hADSCs coupled with HEP14/PLGA microspheres enhanced ovarian regeneration and functional restoration in POI mice

To investigate the therapeutic effects of h-hADSCs alone or in combination with HEP14/PLGA[18] microspheres on doxorubicin-induced POI in mice, we established a POI model using single intraperitoneal injections of three doxorubicin doses (8 mg/kg, 12 mg/kg, and 16 mg/kg). The 16 mg/kg dose caused significant weight loss and poor health in 2 out of 6 mice within 4 weeks, leading to euthanasia. In contrast, the 8 mg/kg and 12 mg/kg doses did not induce such severe effects. Histopathological analysis showed minimal ovarian changes with 8 mg/kg doxorubicin, while 12 mg/kg resulted in pronounced ovarian atrophy and up to 80% follicular degeneration by 4 weeks post treatment, along with significant hormonal imbalances and abnormal estrous cycles (Fig. S3A–F). Therefore, a single 12 mg/kg doxorubicin injection was selected to induce POI. Liquid chromatography-mass spectrometry (LC/MS) analysis was performed to confirm that no HEP14 residues were present in the saline containing h-hADSCs (Fig. S3G). Preliminary experiments indicated that HEP14 alone did not significantly improve ovarian structure or function in POI and aging mice, as evidenced by Hematoxylin & Eosin (H&E) staining and serum hormone levels (Fig. S4A–C). Based on these findings, mice were divided into four groups for the subsequent study: normal control (CTL), POI mice

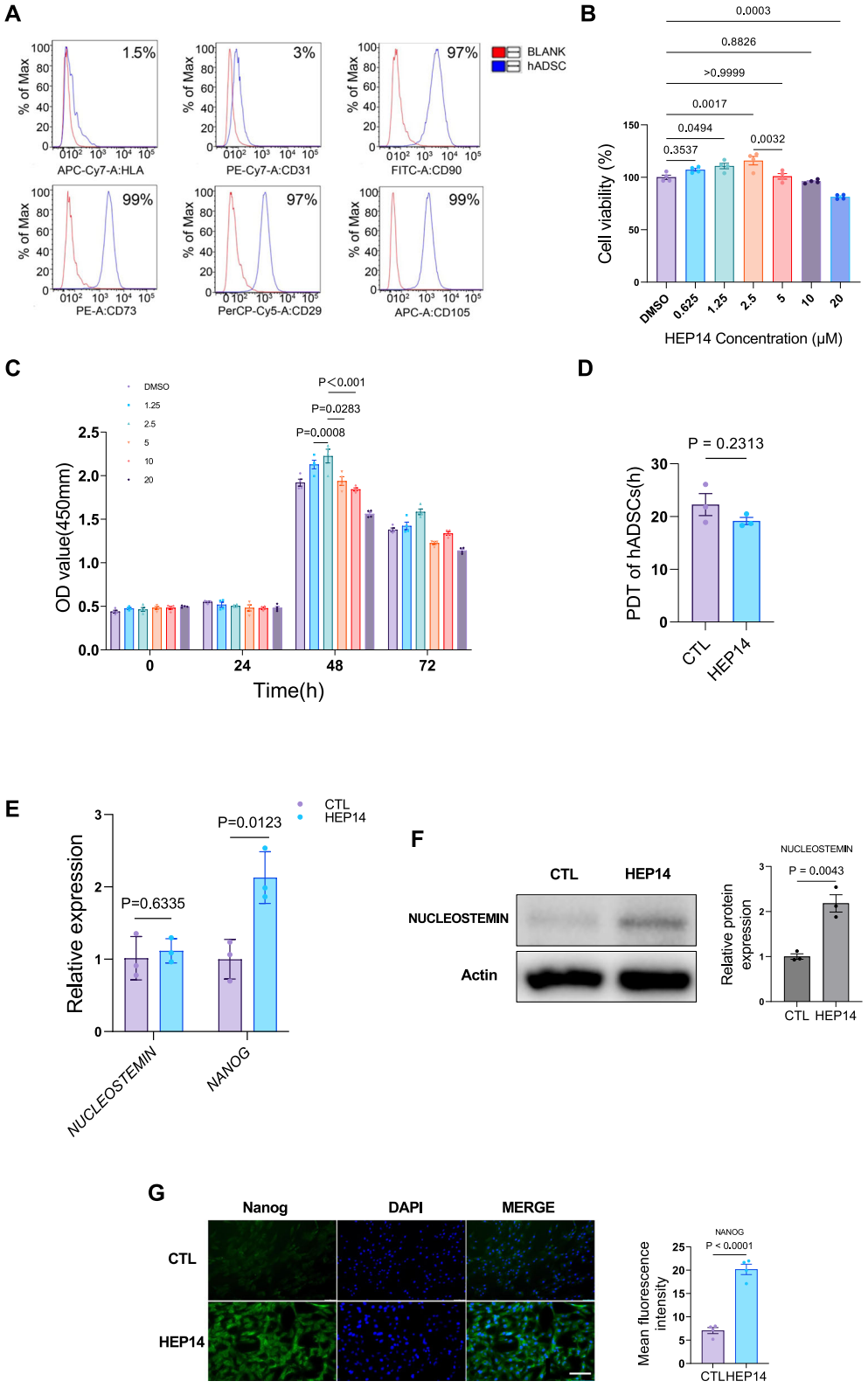

Fig. 1 | Enhanced viability and stemness of primary hADSCs after HEP14 treatment. **A** Surface markers of hADSCs by flow cytometry. **B** Cell viability was measured by CCK8 assay. **C** Effect of HEP14 on hADSC proliferation was determined by CCK8 assay. **D** Population doubling time (PDT) of vehicle-treated hADSCs as control and HEP14-treated hADSCs. **E** mRNA expression of *NUCLEOSTEMIN* and *NANOG* by real-time qPCR. **F** NUCLEOSTEMIN expression and quantification by western blot. **G** NANOG protein levels of by IF staining and quantification in vehicle-treated hADSCs and HEP14-treated hADSCs 48 h post-HEP14 treatment. A HEP14 concentration of 2.5 μM was used in (**D** to **G**). Data are means ± SEM, $n = 3$, except for $n = 4$ in (**B**) and (**C**). *P* values calculated by one-way ANOVA, followed by Tukey-Kramer test in (**B**) and (**C**); *P* values determined by unpaired two-tailed Student's *t*-test in (**D** to **G**). Changes were considered statistically significant when $P < 0.05$. Scale Bar, 100 μm.

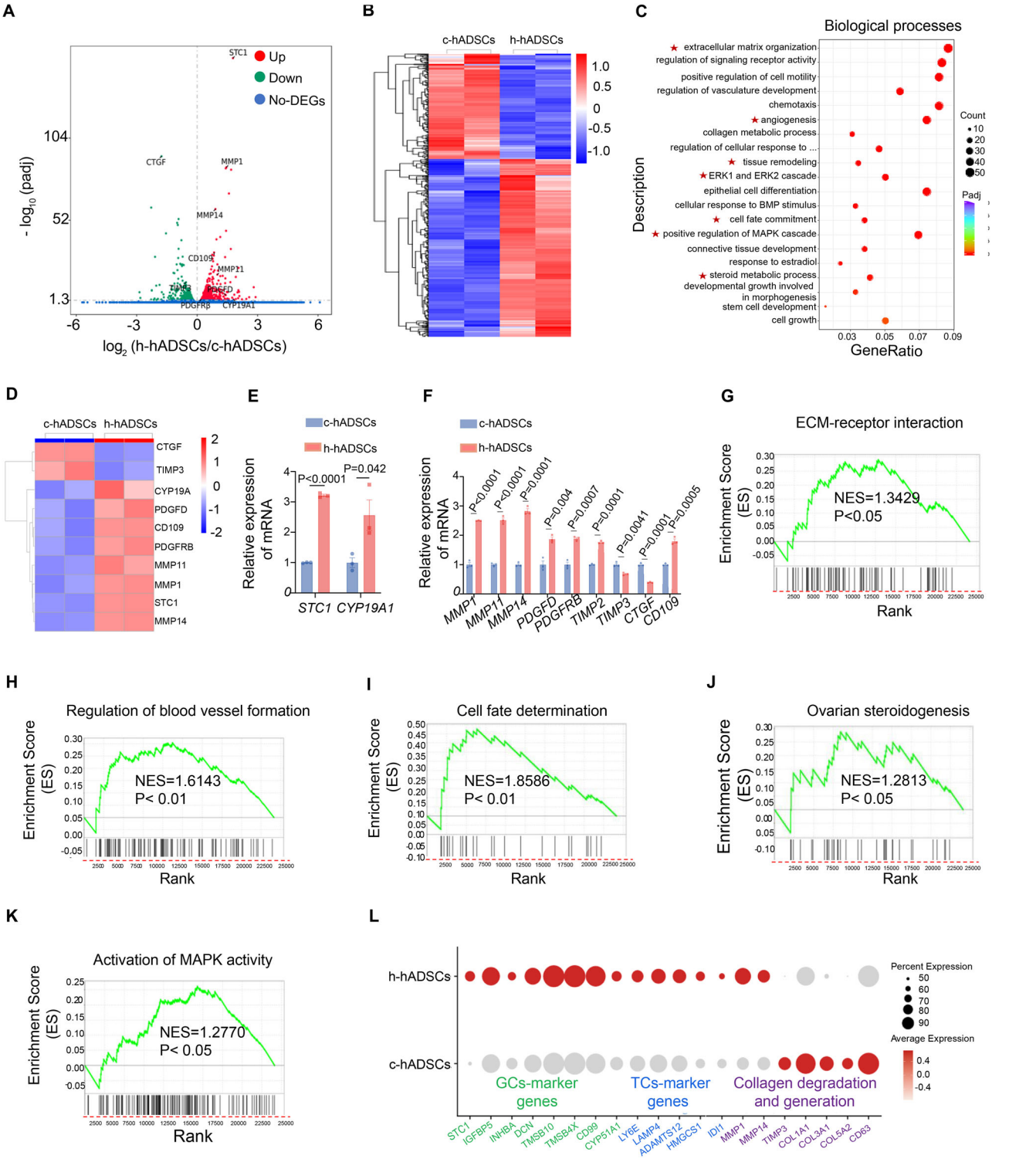

Fig. 2 | Molecular characterization of h-hADSCs at transcriptome levels. **A** Volcano plot showed the differentially expressed genes (DEGs) between h-hADSCs and c-hADSCs. DEGs were identified according to the criteria: |log2FC|> 1 and adj $p < 0.05$. **B** Heat map of DEGs in h-hADSCs and c-hADSCs. **C** 30 enriched terms of DEGs for the biological processes were analyzed by clusterprofiler 3.8.1. **D** Sub-heatmap of the key DEGs by clusterprofiler 3.8.1. **E**, **F** mRNA expression levels of the key DEGs by real-time qPCR. **G**–**K** GSEA analysis was conducted to evaluate the influence of HEP14 on GO and KEGG pathways by gsea v4.0. ECM-receptor interaction (**G**). Regulation of blood vessel formation (**H**). Cell fate determination (**I**). Ovarian steroidogenesis (**J**). Activation of MAPK activity (**K**). **L** Dotplot displayed expression levels of representative key genes for ovarian granulosa, theca cells and tissue remodel in h-hADSCs and c-hADSCs. Data are means ± SEM, $n = 3$. P values determined by unpaired two-tailed Student's t-test in (**E**) and (**F**). Changes were considered statistically significant when $P < 0.05$.

treated with saline (POI), POI mice treated with h-hADSCs alone (h-hADSCs mice), and POI mice treated with the combined therapy of h-hADSCs via intraovarian injection and HEP14/PLGA microspheres via intraperitoneal injection (h-hADSCs/HEP14 mice) (Fig. 3A). Compared with POI mice, both groups treated with h-hADSCs and h-hADSCs/HEP14 exhibited signs of ovarian recovery at 2 and 4 weeks post treatment, with the group treated with h-hADSCs/HEP14 demonstrating better outcomes. This was evidenced by representative images and quantitative measurements of

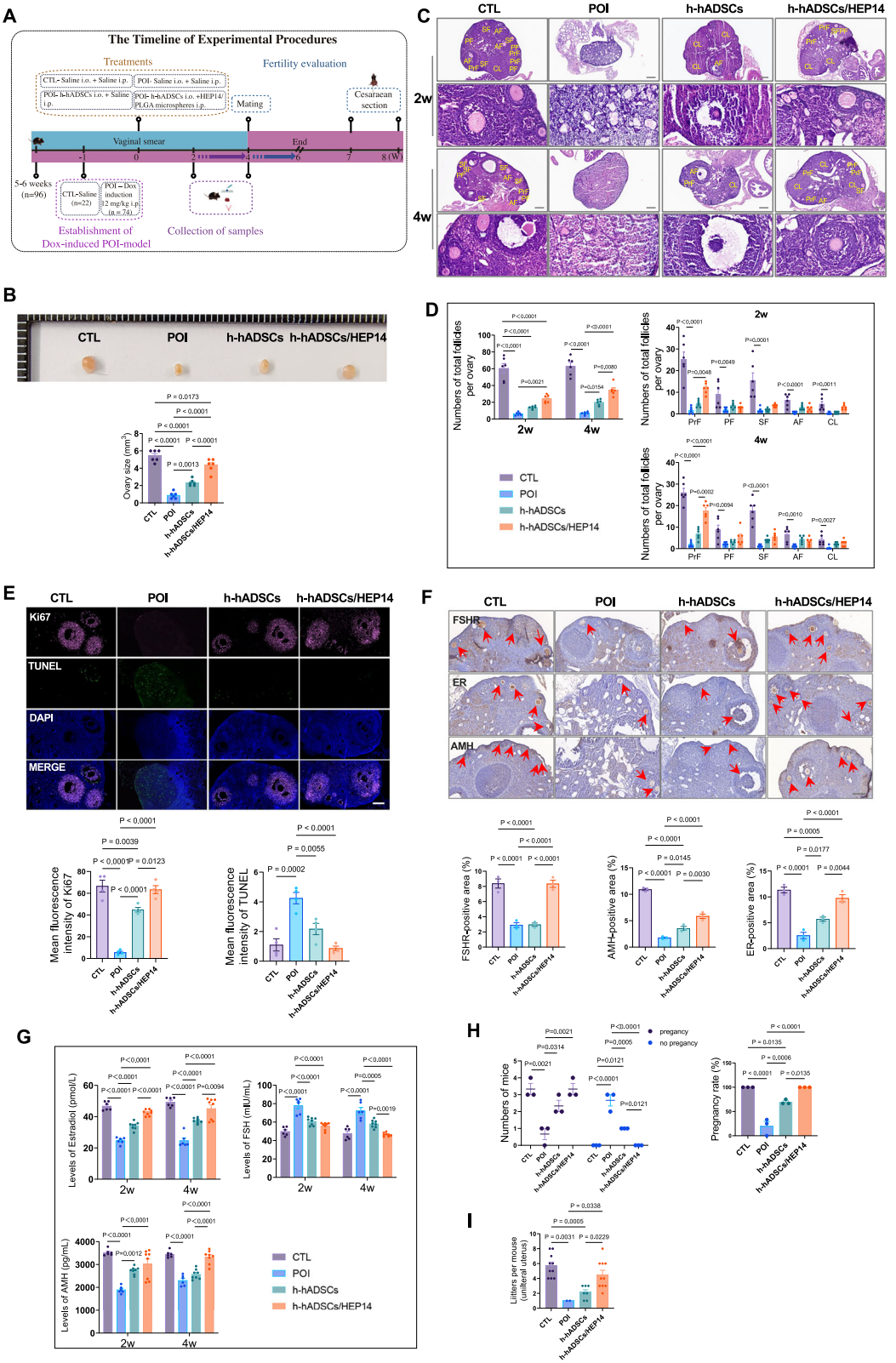

ovarian size (Fig. 3B). Additionally, the h-hADSCs/HEP14 mice had a higher abundance of healthy follicles than the h-hADSCs mice, and the h-hADSCs mice still had significantly more follicles than the POI mice (Fig. 3C and D). Ki67 and TUNEL staining revealed increased proliferation and decreased apoptosis in treated ovaries, particularly in h-hADSCs/HEP14 mice (Fig. 3E). IHC staining revealed higher expressions of FSHR, ERβ, and AMH in treated ovaries, with h-hADSCs/HEP14 mice showing nearly normal levels (Fig. 3F). Hormonal analysis revealed significantly higher E2 and AMH levels but lower FSH levels in h-hADSCs/HEP14 mice and h-hADSCs mice compared to POI mice, with h-hADSCs/HEP14 mice nearly matching normal controls (Fig. 3G). Estrous cycle evaluation showed that most h-hADSCs/HEP14 and h-hADSCs mice regained regular cycles,

Fig. 3 | Combined therapy exhibits superior therapeutic efficacy in promoting ovarian regeneration and restoring ovarian function in POI mice. A Timeline of experimental procedures. **B** Comparison of ovarian size among four groups of normal control mice (CTL), vehicled-treated (POI)-, h-hADSCs-treated (h-hADSCs)-, and h-hADSCs/HEP14-treated (h-hADSCs/HEP14) POI mice at 4 weeks post-treatment. **C** Morphological changes of ovaries from four groups of POI mice at 2 weeks and 4 weeks post-treatment, assessed by H&E staining (annotations indicate follicles, PrF, primordial follicle; PF, primary follicle; SF, secondary follicle; AF, antral follicle; CL, Corpus Luteum). **D** Comparison of total follicle count and follicle numbers at various developmental stages in the right ovaries from four groups of POI mice, assessed at 2 weeks and 4 weeks post-treatment. **E** IF staining of ovarian sections with Ki67 and TUNEL, and quantification of fluorescence intensity for Ki67 and TUNEL among four groups at 4 weeks post-treatment. **F** IHC staining of ovarian sections demonstrating the expression of FSHR, ERβ, and AMH in the ovaries of four groups at 4 weeks post-treatment (arrows indicate positive expression areas of FSHR, ERβ, and AMH in follicles of different stages). **G** Comparison of serum E2, FSH, and AMH levels among four groups at 2 weeks and 4 weeks post-treatment. **H** Pregnancy rates among four groups. **I** Total number of litters per mouse delivered via cesarean section from the right side of the uterus, corresponding to the treated ovaries from four groups. Data are presented as means ± SEM. Sample sizes: $n = 6$ for (**B** to **D**), $n = 3$-4 for (**G**), $n = 4$ for (**E**), $n = 3$ for (**F**), and $n = 10$ in (**H**), $n = 10$ for CTL and h-hADSCs/HEP14, $n = 2$ for POI, and $n = 7$ for h-hADSCs groups in (**I**). *P* values were calculated by one-way ANOVA, followed by Tukey-Kramer post hoc test. Changes were considered statistically significant when $P < 0.05$. Scale bar = 200 μm.

unlike POI mice which showed prolonged cycles (Fig. S4D). Overall, both therapies enhanced ovarian regeneration and restored endocrine function in POI mice, with the combined therapy outperforming the standalone h-hADSCs therapy.

Four weeks post-treatment, mating trials revealed that pregnancy rates and litter sizes from the right side of treated ovaries were illustrated in Fig. 3H and Fig. 3I. POI mice had a significantly low pregnancy rate (2/10) compared to 7/10 in h-hADSCs mice, 10/10 in h-hADSCs/HEP14 mice, and 10/10 in controls via cesarean section (Fig. 3H). POI mice averaged only one fetus per litter, significantly lower than the 2.1, 4.6, and 5.7 fetuses observed in h-hADSCs, h-hADSCs/HEP14, and control mice, respectively (Fig. 3I). Interestingly, the h-hADSCs/HEP14 group witnessed a case of monozygotic twins (Fig. S4E), suggesting superior fertility outcomes with the combined therapy compared to the standalone h-hADSCs therapy. Collectively, these results indicate that both h-hADSCs and combined therapies effectively promoted ovarian fertility restoration in POI mice, with the combined therapy demonstrating more effective than the standalone h-hADSCs therapy.

h-hADSCs coupled with HEP14/PLGA microspheres substantially improved ovarian endocrine function in aging mice

We further assessed the therapeutic efficacy of h-hADSCs and h-hADSCs/HEP14 in 12-month-old aging mice, a model representing human ages 40 ~ 42[22]. These aging mice were administered h-hADSCs, h-hADSCs/HEP14, or saline, and were subsequently categorized as h-hADSCs aging mice, h-hADSCs/HEP14 aging mice, and control aging mice, respectively. Histopathological examination revealed that ovaries from both h-hADSCs/HEP14- and h-hADSCs aging mice were larger than controls, with h-hADSCs/HEP14 aging ovaries being the largest (Fig. 4A). Ovaries from h-hADSCs/HEP14 aging mice also contained more follicles at various stages compared to h-hADSCs aging mice, while control aging ovaries showed predominantly atretic follicles (Fig. 4B and C). IHC staining revealed higher FSHR, ERβ, and AMHR2 expressions in treated groups, with h-hADSCs aging ovaries showing intermediate levels (Fig. 4D). PCNA and TUNEL staining demonstrated increased proliferation and reduced apoptosis in treated ovaries, particularly in h-hADSCs/HEP14 aging mice (Fig. 4E). Hormonal analysis demonstrated that, compared to the controls, both the h-hADSCs/HEP14-treated and h-hADSCs-treated aging mice exhibited markedly increased serum concentrations of E2, AMH, inhibin-A (INH-A), and inhibin-B (INH-B), along with decreased levels of FSH (Fig. 4F and G). Notably, E2, AMH and FSH serum hormone levels in the h-hADSCs/HEP14 aging mice more closely resembled those of control young mice than those in the h-hADSCs aging mice (Fig. 4F). These findings indicate an enhancement in endocrine function in both h-hADSCs/HEP14 and h-hADSCs aging mice compared to those in control young mice. Additionally, most h-hADSCs/HEP14 aging mice regained regular estrus cycles, unlike h-hADSCs aging mice with irregular cycles and control aging mice lacking estrus (Fig. 4H). In conclusion, both treatments appear to improve ovarian function in aging mice, with the combined therapy demonstrating better therapeutic efficacy.

HEP14 enhances retention, anti-fibrotic and pro-angiogenic effects, and promotes transdifferentiation of h-hADSCs

Transplanted h-hADSCs labeled with CM-Dil or QTracker dyes were traced using a human-specific anti-vimentin antibody, which demonstrated no cross-reactivity with mouse tissues, ensuring specific detection of the transplanted cells. IF staining confirmed the presence of these transplanted cells within the ovaries by demonstrating co-localization of vimentin staining with the cell tracker signals (Fig. 5A and B). At four weeks post-transplantation, we observed significant engraftment of labeled h-hADSCs in the ovaries. Specifically, ovaries treated with h-hADSCs/HEP14/PLGA exhibited extensive integration of h-hADSCs into both the follicular granulosa and theca layers. In contrast, ovaries from POI or aging mice treated with h-hADSCs alone showed minimal integration, primarily confined to the theca layers (Fig. 5A and B). These results indicate that intraperitoneal injection of HEP14/PLGA microspheres enhances h-hADSCs retention, survival, and transdifferentiation.

Picrosirius red (PSR) staining and polarized microscopy revealed thinner, uniformly distributed collagen fibrils in normal ovaries, whereas thicker, clustered fibrils were observed in POI and aging ovaries. Masson trichrome staining demonstrated a higher abundance of collagen fibers (stained blue) in POI and aging ovaries, thereby indicating an elevated collagen content in POI and aging ovaries compared to the treated groups (Fig. 5C and D; Fig. S5A and B). Treatment with either h-hADSCs/HEP14 or h-hADSCs alone reduced the thickness and clustering of these fibrils (Fig. 5C and D). IHC and IF staining showed that h-hADSCs/HEP14 treatment decreased the expression of α-SMA, a marker of fibrosis[23], and increased the expression of CD31, an endothelial cell marker[24], in POI (Fig. 5E and F) and aging ovaries (Fig. 5G and H) compared to untreated ovaries, which exhibited higher α-SMA and lower CD31 levels. Mice treated with h-hADSCs alone showed intermediate effects (Fig. 5E–H). The results indicate that intraperitoneal injection of HEP14/PLGA microspheres facilitates the improvement of the ovarian microenvironment by enhancing the anti-fibrotic and pro-angiogenic effects of h-hADSCs. Collectively, these findings demonstrate that HEP14 enhances the therapeutic efficacy of h-hADSCs by improving the ovarian microenvironment, promoting the retention and transdifferentiation of h-hADSCs, thereby leading to ovarian regeneration and functional restoration in POI and aging mice.

HEP14-activated PKC-ERK1/2-MMP1 and -PDGFD pathways enhanced anti-fibrotic and pro-angiogenic effects of h-hADSCs

To elucidate the mechanisms underlying the anti-fibrotic and pro-angiogenic effects of h-hADSCs by HEP14, we investigated the involvement of the PKC-ERK1/2-MMP1 and PDGFD signaling pathways by the use of specific PKC and ERK1/2 inhibitors. Western blot analysis confirmed that HEP14 treatment activated PKC and ERK1/2 phosphorylation in HEP14-treated hADSCs (Fig. 6A) and significantly increased the expression of MMP1, PDGFD, and PDGFRβ compared to vehicle-treated hADSCs (Fig. 6B). These effects were reversed by the PKC inhibitor (Bis I) and the ERK1/2 inhibitor (PD98059) in hADSCs treated with either HEP14+Bis I or HEP14 + PD98059 (Fig. 6A and B). IHC and double IF staining revealed higher expression levels of pPKC, pERK1/2, MMP1, PDGFD, and PDGFRβ

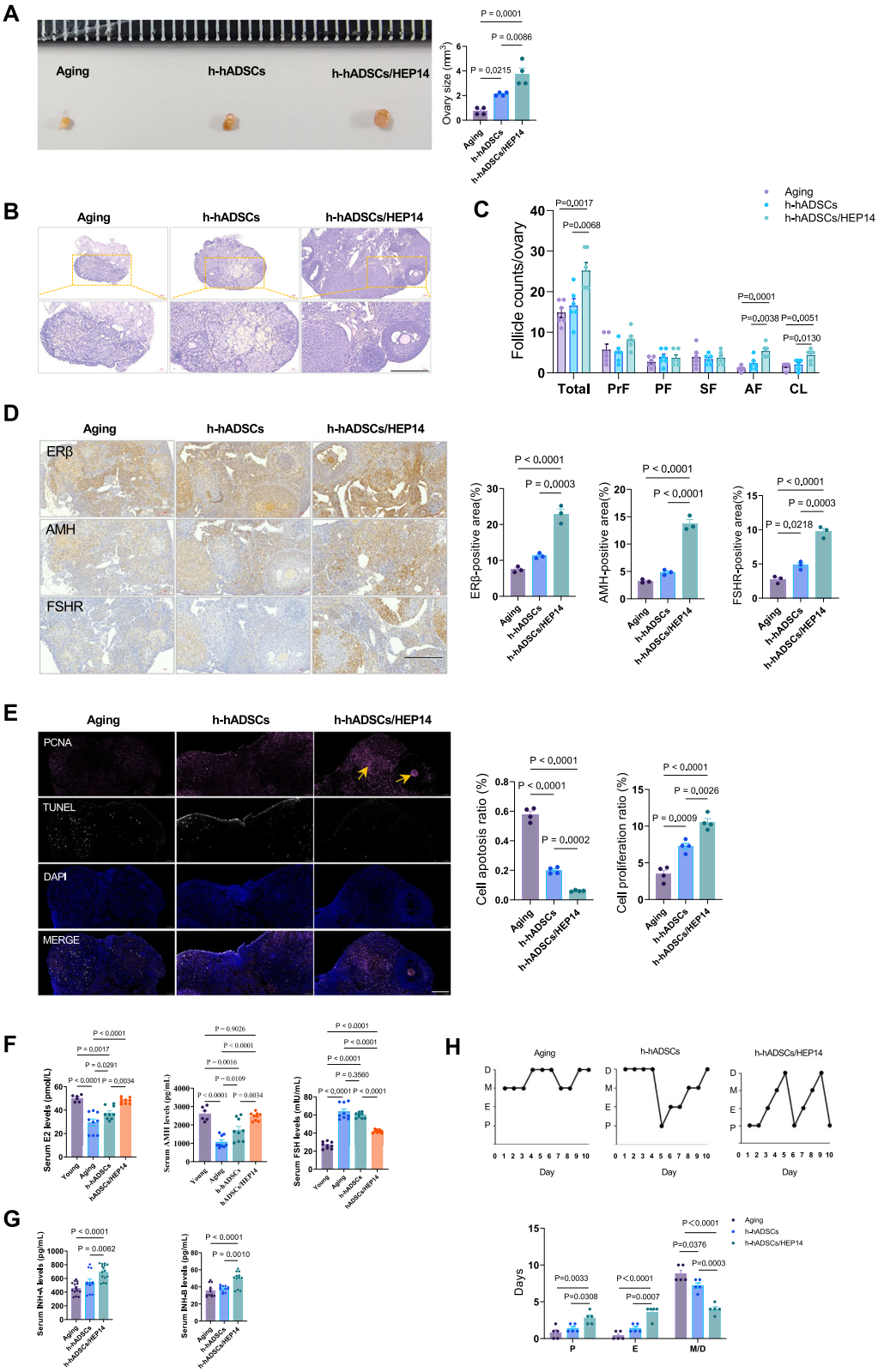

in ovaries treated with h-hADSCs/HEP14 compared to those treated with h-hADSCs alone and controls in both POI (Fig. 6C and D) and aging mice (Fig. 6E and F). Expression levels in the h-hADSCs groups were intermediate. No significant differences were observed between h-hADSCs/HEP14 ovaries and control ovaries in POI and aging mice (Fig. 6C–F). Together, these data indicate that HEP14 enhances the antifibrotic and proangiogenic effects of h-hADSCs via the HEP14-PKC-ERK1/2-MMP1 and -PDGFD pathways.

To further validate these findings, we collected conditioned media (CM) from hADSCs cultured under various treatments. Specifically, we obtained CM from hADSCs treated with vehicle only (c-hADSCs-CM), with HEP14 alone (h-hADSCs-CM), with a combination of HEP14 and

Fig. 4 | Combined therapy demonstrates superior therapeutic efficacy in ovarian regeneration and functional restoration in aging mice. **A** Comparison of ovarian size among three groups of aging ovaries in vehicle-treated- (as control)-, h-hADSCs-treated (h-hADSCs)-, and h-hADSCs/HEP14-treated (h-hADSCs/HEP14) aging mice at 4 weeks post-treatment. **B** Morphological changes in three groups of aging ovaries in mice with ARNA-OI at 4 weeks post-treatment, assessed by H&E staining. **C** Comparison of total follicle count and follicle numbers at various developmental stages among the three groups of aging ovaries. **D** IHC staining of ovarian sections demonstrating the expression of FSHR, ERβ, and AMH in the three groups. **E** IF staining of ovarian sections with PCNA and TUNEL, and quantification of fluorescence intensity for PCNA and TUNEL in the three groups (arrows indicate proliferating granulosa cells and follicles). **F** Comparison of serum E2, AMH, FSH, levels among the four groups of young-, aging-, h-hADSCs-treated (h-hADSCs)-, and h-hADSCs/HEP14-treated (h-hADSCs/HEP14) aging mice. **G** Comparison of serum INH-A and INH-B levels among the three groups of aging-, h-hADSCs-treated aging (h-hADSCs)-, and h-hADSCs/HEP14-treated (h-hADSCs/HEP14) aging mice. **H** Evaluation of estrous cycles in the three groups. Data are presented as means ± SEM. Sample sizes: $n = 6$ for (**A** to **C**); $n = 3$ for (**D** to **G**) and $n = 5$ for (**G**). P values were calculated by one-way ANOVA, followed by Tukey-Kramer post hoc test. Changes were considered statistically significant when $P < 0.05$. Scale bar = 100 μm.

PKC inhibitor Bis I (h-hADSCs+PKCi-CM), or with a combination of HEP14 and an ERK1/2 inhibitor PD98059 (h-hADSCs+ERKi-CM). ELISA analysis confirmed that HEP14 increased MMP1 secretion in h-hADSCs-CM compared to c-hADSCs-CM (Fig. 6G). This increase was effectively reversed by Bis I and PD98059, confirming the involvement of the PKC-ERK1/2 signaling pathway in HEP14-induced MMP1 secretion. Next, we assessed the angiogenic potential of these CMs using human umbilical vein endothelial cells (HUVECs). HUVECs were cultured with the various CMs and a PDGFD neutralizing antibody (PDGFD Nab). The results showed that h-hADSCs-CM significantly enhanced tube formation in HUVECs compared to c-hADSCs-CM, as evidenced by increased total tube length and branching points (Fig. 6H). This pro-angiogenic effect was nearly abolished by h-hADSCs+PKCi-CM, h-hADSCs+ERKi-CM, and PDGFD Nab, indicating that the enhanced tube formation was mediated by HEP14-activated PKC-ERK1/2 pathway and PDGFD secretion. IF staining for CD31 further corroborated these findings (Fig. 6I). Collectively, these data demonstrate that the co-administration of h-hADSCs with HEP14/PLGA microspheres enhances the secretion of MMP1, PDGFD and PDGFRβ via the HEP14-activated PKC-ERK1/2 signaling pathway. This enhancement significantly augments the anti-fibrotic and pro-angiogenic effects of the combined therapy, thereby improving the ovarian microenvironment and promoting follicular regeneration in POI and aging mice.

The transdifferentiation of h-hADSCs mediated by HEP14-PKC-ERK1/2-STC1-CYP19A1 promoted ovarian regeneration and functional restoration

In parallel, we investigated the signaling mechanisms underlying the efficacy of combined therapy in promoting ovarian follicular regeneration and endocrine function. Guided by RNA-seq analysis data, we focused on the roles of STC1 and CYP19A1, which are expressed in ovarian GCs. Western blot analysis validated that HEP14 increased the expression levels of STC1 and CYP19A1 in HEP14-treated hADSCs compared to those in vehicle-treated hADSCs (Fig. 7A). Co-culture with either the PKC inhibitor Bis I or the ERK1/2 inhibitor PD98059 abrogated these effects, indicating that HEP14 upregulates STC1 and CYP19A1 via the PKC-ERK1/2 signaling pathway (Fig. 7A). In vivo, IHC staining revealed higher STC1 expression in h-hADSCs/HEP14 and h-hADSCs ovaries compared to controls, with intermediate expression in h-hADSCs ovaries in both POI and aging mice (Fig. 7B and C). Triple IF staining showed overlapped vimentin signals in transplanted h-hADSCs with FSHR (a marker for ovarian cells) and CYP19A1 (a marker for granulosa cells) in GC layers[25,26], and FSHR and CYP17A1 (a marker for theca cells)[26] in TC layers, in h-hADSCs/HEP14 ovaries of POI mice (Fig. 7D and E) and aging mice (Fig. 7F and G). This suggests transdifferentiation of h-hADSCs into functional GC-like and TC-like cells. To further validate STC1's regulation of CYP19A1, we conducted a knockdown experiment in KGN cells[27,28]. Suppression of STC1 by specific siRNA reduced CYP19A1 expression (Fig. 7H), confirming STC1's regulatory role. Collectively, our findings indicate that the combined therapy facilitates h-hADSC transdifferentiation into functional GC-like and TC-like cells via the PKC-ERK1/2-STC1-CYP19A1 pathway, thereby promoting follicular regeneration, development, and restoring endocrine function in POI and aging mice.

Discussion

MSCs, particularly hADSCs, play a pivotal role in the regeneration of injured tissues[13], making them a promising therapeutic option for the treatment of OI. Our in vitro findings revealed that HEP14 enhances the viability and stemness of h-hADSCs, modulates their gene expression profiles, and predisposes these cells to transdifferentiate into ovarian cells at the transcriptomic level. In our in vivo study, we introduced an innovative approach where h-hADSCs were administered via o.i. injection, coupled with HEP14/PLGA microspheres via i.p. injection. Remarkably, we observed more pronounced ovarian regeneration and functional restoration in the ovaries of mouse models of POI and ARNA-OI that received the h-hADSCs/HEP14 combination therapy, compared to those that received only h-hADSCs. These improvements were attributed to the enhancement of anti-fibrotic and pro-angiogenic effects, as well as the improved retention and transdifferentiation of h-hADSCs into ovarian cells. Mechanistically, the marked upregulation of key genes, including MMP1, PDGFD, and STC1 by HEP14-activated PKC-ERK1/2 signaling pathways, were tightly involved in the improved biologic processes leading to ovarian regeneration. It is important to note that other relevant pathways, such as PI3K-AKT and Wnt/β-catenin, also play important roles in the proliferation, apoptosis, and differentiation of ovarian granulosa cells[29–31]. For example, PI3K-AKT activation enhances cell survival and reduces apoptosis, potentially complementing the anti-fibrotic and pro-angiogenic effects observed in our study. Meanwhile, Wnt/β-catenin signaling can promote the differentiation of stem cells into specific cell types, potentially enhancing the transdifferentiation of h-hADSCs into ovarian cells. Future studies should explore the interplay between the HEP14-activated PKC-ERK1/2 pathway and these other pathways to better understand their combined effects on ovarian regeneration. This is the first report demonstrating the transdifferentiation of h-hADSCs into functionally active ovarian cells in vivo. To our knowledge, this therapeutic strategy represents a novel intervention in the treatment of POI and aging mouse models. This finding holds profound implications for the advancement of therapeutic strategies for OI and its associated complications, potentially paving the way for new treatment options in the future.

Doxorubicin, a prevalent first-line chemotherapeutic and adjuvant therapy[32], was used to establish a mouse model of POI. This treatment caused ovarian tissue damage, substantially reducing the follicular pool, and inducing fibrous tissue growth and collagen deposition. A 12-month-old mouse is physiologically comparable to a 40~42-year-old human[22]. As mice age and undergo ovarian cycles, ovarian fibrosis develops, marked by fibrous tissue growth and collagen deposition[33,34]. This fibrosis, a fundamental pathological change from chemotherapy or aging, leads to reduced tissue receptivity and ischemia, grafted cell loss, ultimately causing cell treatment failure[35]. Successful ovarian tissue regeneration critically hinges on key triad elements: the ovarian microenvironmental cues that guide cell growth and differentiation, the vital role of transplanted h-hADSCs in regeneration (including their activity, number, and secreted proteins), and the intricate structural characteristics of the ovary along with its inherent limitations on transplant acceptance in damaged and aging ovaries. Modulation of PKC pathway is a recognized strategy for physiologically modifying cells[15]. In this study, distinct administration routes were adopted for h-hADSCs and HEP14/PLGA microspheres. This approach allowed for the

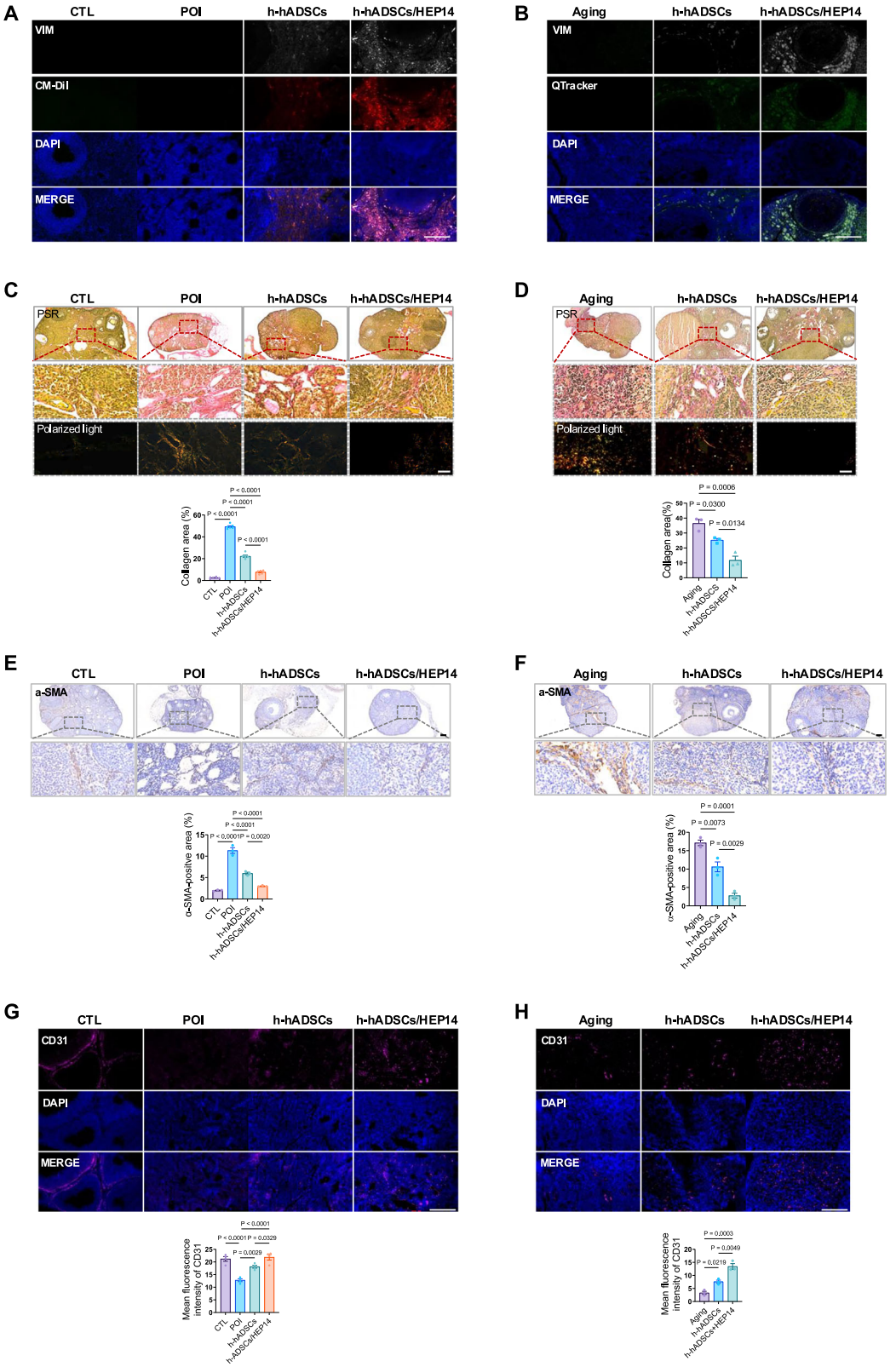

accommodation of a larger volume of transplanted h-hADSCs, enabling them to adapt directly to the dynamic ovarian microenvironment and facilitating interactions among HEP14, h-hADSCs, follicles, secreted proteins by h-hADSCs, and the ECM. Consequently, embedding h-hADSCs within h-hADSCs/HEP14 ovaries significantly enhanced their therapeutic efficacy, enabling them to play a more efficacious role in treating POI and ARNA-OI in mice. PLGA, with its long history of safe human use and tunable biodegradation rate, has been widely recognized, with twelve PLGA-based microsphere drug products approved by the U.S. FDA[16,17]. However, it is important to note that the murine model may not fully replicate the complexity of POI and ARNA-OI in humans. Therefore, it is crucial to validate the efficacy and safety of our therapeutic approach in diverse populations and models. When comparing HEP14 to other PKC activators such as bryostatin, distinct profiles in both efficacy and safety emerge.

Fig. 5 | HEP14 enhances h-hADSC-mediated anti-fibrotic, pro-angiogenic, retention, and transdifferentiation effects in POI and aging ovaries. **A** Representative IF-stained ovarian sections showing vimentin co-localized with CM-Dil in four groups of normal control ovaries, vehicle-treated (POI)-, h-hADSCs-treated (h-hADSCs)-, and h-hADSCs/HEP14-treated (h-hADSCs/HEP14) POI ovaries from POI mice at 4 weeks post-treatment. **B** Representative IF-stained ovarian sections showing Vimentin co-localized with QTracker in three groups of control aging (aging)-, h-hADSCs-treated (h-hADSCs)- and h-hADSCs/HEP14-treated (h-hADSCs/HEP14) aging ovaries in mice with ARNA-OI. **C** PSR-stained ovarian sections and quantification of fibrotic areas in four groups of POI ovaries. Polarized light microscopy images depict collagen I (red) and collagen III (green) fibrils. **D** PSR-stained ovarian sections and quantification of fibrotic areas in three groups of aging ovaries. Polarized light microscopy images depict collagen I (red) and collagen III (green) fibrils. **E** Representative IHC images of α-smooth muscle actin (α-SMA) and quantification in four groups of POI ovaries. **F** Representative IHC images of α-SMA and quantification in three groups of aging ovaries. **G** Representative IF-stained images of CD31 and quantification in four groups of POI ovaries. **H** Representative IF-stained images of CD31 and quantification in three groups of aging ovaries. Data are presented as means ± SEM. $n = 6$ for (**C**), $n = 3$ for (**D**), $n = 3$ for (**E** to **F**) and (H), $n = 4$ for (**G**). P values were calculated by one-way ANOVA, followed by Tukey-Kramer post hoc test. Changes were considered statistically significant when $P < 0.05$. Scale bar = 100 μm.

Bryostatin is known for its anticancer effects across multiple cancer types and its role in aiding Alzheimer's cognition through the activation of PKC δ/ε. However, it exhibits a dose-dependent safety profile in Alzheimer's trials and is highly toxic in some cancer trials[36]. In contrast, HEP14 selectively activates PKCα/δ[11]. This selectivity may help reduce adverse reactions, thereby potentially enhancing the therapeutic efficacy and safety profile of HEP14. Nevertheless, the clinical efficacy and safety of HEP14 remains unclear due to limited current data, highlighting the need for further investigation. To facilitate the clinical translation of HEP14, our future work should focus on optimizing cell preconditioning strategies, establishing standardized protocols, and conducting long-term follow-up studies. By addressing these challenges effectively, we can advance the clinical translation of this treatment strategy for managing POI and ARNA-OI.

Ovarian regeneration is a complex and dynamic process, relying on intricate mechanisms of tissue remodeling, angiogenesis, and cell proliferation. Bulk RNA-seq analysis revealed that HEP14 modulated the transcriptomic landscape of h-hADSCs. The most prevalent GO terms in the biological process category and GSEA analysis associated with DEGs were related to ECM organization, angiogenesis, tissue remodeling, cell fate determination, and ERK1/2 signaling cascades. The scRNA-seq data provided additional support that h-hADSCs highly expressed representative key genes for ovarian granulosa cells and theca cells compared with c-hADSCs, indicating that HEP14 may prime h-hADSCs for transdifferentiation into ovarian-like cells. These findings are pivotal in facilitating ovarian tissue regeneration. The key DEGs intricately involved in this process in h-hADSCs include MMP1, PDGFD, and STC1. These genes encode proteins that exert distinct functions: MMP1 catalyzes the degradation of collagen types I, II, and III, modifying the tissue microenvironment to foster regeneration[37,38]; PDGFD, a potent angiogenic growth factor, stimulates angiogenesis through its interaction with PDGFRβ[39] and STC1, a peptide hormone, modulates the differentiation of granulosa cells[40,41]. Collectively, our findings uncover a previously unreported result that HEP14 has the capacity to reset the transcriptional pattern of h-hADSCs, promoting ovarian tissue remodel.

The reduction of collagen deposition within the ovarian stroma is essential for promoting ovarian regeneration[42,43]. In vivo studies revealed a marked upregulation of Mmp1, Pdgfd, Pdgfrβ, Stc1 and CD31 alongside a downregulation of collagen fibril and α-SMA in h-hADSC/HEP14- and h-hADSCs ovaries, compared to control ovaries from both POI and aging mice. h-hADSCs ovaries exhibited intermediate levels of collagen fibril content and gene expression. MMP1 was one of the most highly expressed DEGs in h-hADSCs, and ELISA assay results further validated that HEP14 increased MMP1 expression in h-hADSCs via the PKC-ERK1/2 signaling pathway. Additionally, HEP14 significantly stimulated the expression of PDGFD and PDGFRβ in h-hADSCs. HUVEC tube formation assays and western blot analysis strongly support that HEP14 enhanced angiogenesis through the HEP14-PKC-ERK1/2-PDGFD signaling pathway. The specificity of this pathway was confirmed by the significant reduction in tube formation induced by h-hADSC-CM upon PDGFD neutralization. Collectively, these findings indicate that h-hADSCs alone or in combination with HEP14/PLGA microspheres foster a more favorable microenvironment for ovarian follicular regeneration. This is accomplished through two distinct mechanisms via the HEP14-PKC-ERK1/2-MMP1 and -PDGFD signaling pathways.

STC1 is the most prominently upregulated DEG in h-hADSCs potentiated by HEP14. Literature indicates that STC1, a peptide hormone, extensively expressed in the granulosa cells of follicles across various species, including rodents, swine, and humans, where it functions as an autocrine or paracrine regulator of follicle development[41,44]. STC1 augments expression of CYP19A1 within granulosa cells[45], thereby catalyzing estradiol production, which is crucial for recruitment theca cells and AMH synthesis[46]. The estradiol-mediated effects in rodent granulosa cells are transduced via the activation of estrogen receptor β (ERβ)[47]. In both POI and ARAN-OI model mice, the expression levels of STC1, CYP19A1, AMH and ERβ were found to be elevated in the h-hADSC/HEP14 ovaries compared to h-hADSCs ovaries. Western blot revealed that the HEP14-activated PKC-ERK1/2 signaling pathway upregulated STC1 expression in h-hADSCs. Additionally, knockdown experiments substantiated that the silencing of STC1 led to a downregulation of CYP19A1 expression in KGN cells. Collectively, these findings underscore the synergistic interplay between the elevated levels of STC1, CYP19A1, and estradiol in promoting the proliferation of granulosa and theca cells through the HEP14-PKC-ERK1/2-STC1 signaling cascade. This highlights the potential therapeutic effects of this combined therapy for the restoration of ovarian function.

To date, the literature on the effects of stem cells in the treatment of ARNA-OI remains limited[48]. Earlier studies have suggested that the therapeutic benefits of MSCs in treating POI is predominantly attributed to paracrine effects; nevertheless, the precise mechanisms are not fully elucidated. Sporadic reports have noted the presence of MSCs in the theca cell layers of follicles following transplantation[49]. In line with these earlier findings, a modest number of h-hADSCs were detected in the interstitial tissues and theca layer of ovarian follicles in POI mice four weeks following h-hADSC transplantation. In contrast, a substantial quantity of transplanted h-hADSCs were found in the ovaries of both POI and aging mice when co-administered with HEP14/PLGA microspheres via i.p. injection. This indicates that intraperitoneal injection of HEP14/PLGA microspheres significantly augmented the retention and proliferation of h-hADSCs within ovaries. Importantly, these transplanted h-hADSCs integrated into granulosa cells or theca cell layers of developing follicles. These incorporated h-hADSCs expressed FSHR, Cyp19A1, and Cyp17A1, implying that they underwent transdifferentiation into granulosa-like or theca-like cells capable of producing E2 and AMH. Consistent with this, the ovarian hormone levels in h-hADSCs/HEP14 mice with ARNA-OI were markedly restored to levels akin to those of young control mice, although the serum levels of ovarian hormones were significantly elevated in the h-hADSCs/HEP14 mice and hADSCs mice compared to untreated POI or aging mice. Furthermore, an inverse correlation between FSH and Inhibin A/B levels was observed in aging mice, indicative of enhanced endocrine function and a rejuvenated ovarian state. Additionally, scRNA-seq analysis results suggest that HEP14 treatment predisposed hADSCs to transdifferentiate into ovarian granulosa/theca cell-like cells. This transdifferentiation is crucial for promoting follicle development and restoring ovarian function. To our knowledge, no previous reports have demonstrated that h-hADSCs directly and substantially differentiate into granulosa cells in vivo.

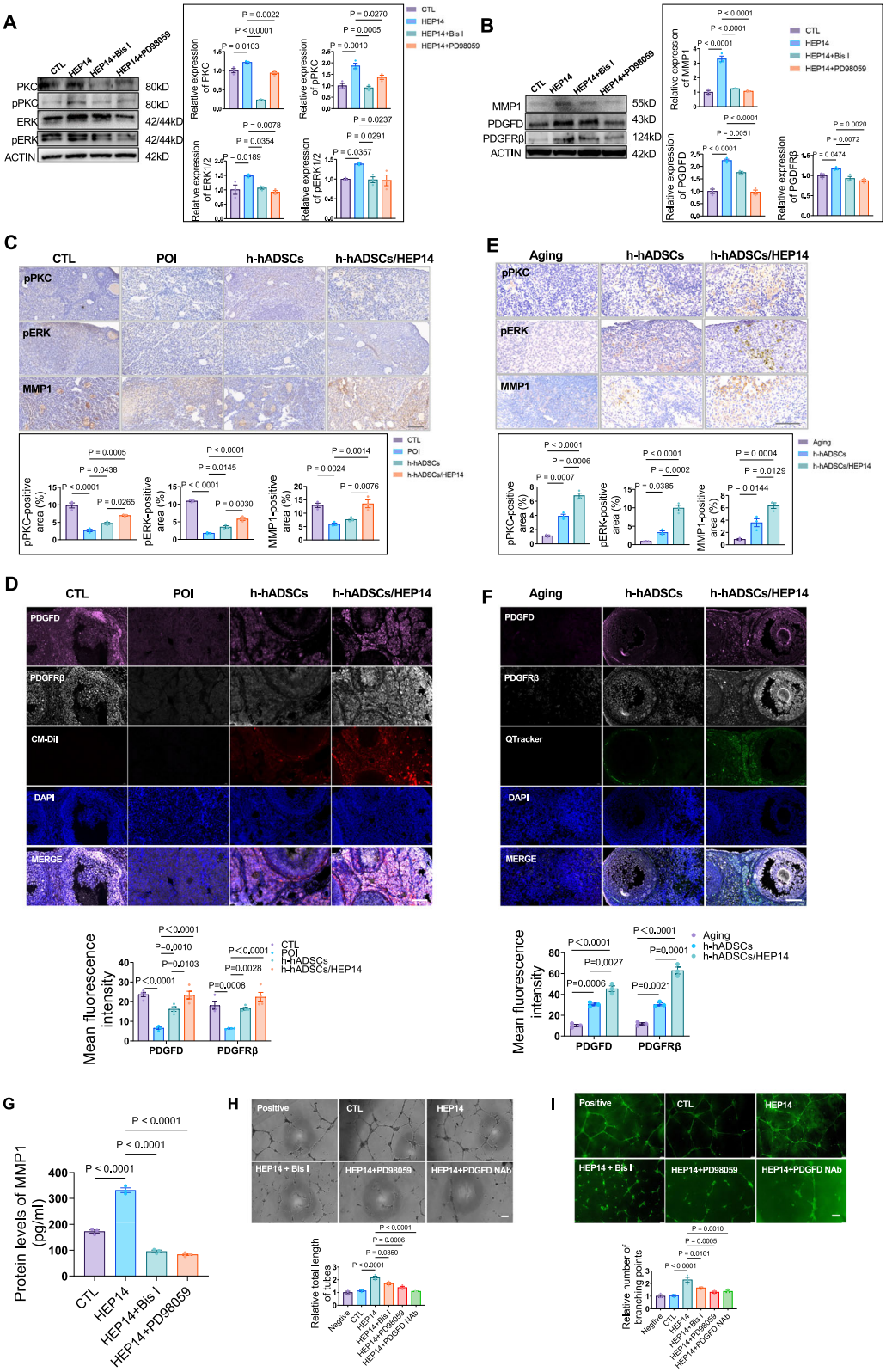

The restoration of fertility stands as a critical metric in evaluating the therapeutic effectiveness for POI. Our findings reveal that h-hADSCs therapy successfully restored fertility in POI mice, and notably, the combined therapy exhibited a markedly enhanced therapeutic effect compared to the h-hADSCs therapy alone, as well as outperforming results previously reported in the literature. Specifically, the combined therapy remarkably increased the pregnancy rate to a normal level of 10 out of 10 in h-hADSC/HEP14 mice, with one case resulting in the birth of monozygotic twins. This outcome contrasts sharply with the pregnancy rates observed in 7 out of 10 h-hADSCs mice, 2 out of 10 untreated POI mice, and the rates reported in other studies. For instance, a 7 out of 9 pregnancy rate was observed in TG-induced POI rats and treated with ADSCs on soluble collagen scaffolds[13], 4 out of 6 in POI mice receiving embryonic stem cell-derived MSCs[50,51], and 3 out of 6 in POI mice administered bone marrow-derived MSCs[50]. Of note,

Fig. 6 | HEP14 intensified the anti-fibrotic and pro-angiogenic effects of h-hADSCs via activating PKC-ERK1/2-MMP1 and -PDGFD signal cascades. **A** Expression and quantification of PKC, pPKC, ERK1/2 and ERK1/2 in h-hADSCs and c-hADSCs by Western blot. **B** Expression and quantification of MMP1, PDGFD and PDGFRβ in HEP14-treated hADSCs and vehicle-treated-hADSCs as control by Western blot. **C** Representative images of IHC-stained ovarian sections and quantification with pPKC, pERK1/2 and MMP1 in four groups of normal control (CTL), vehicle-treated (POI)-, h-hADSCs-treated (h-hADSCs), and h-hADSCs/HEP14-treated (h-hADSCs/HEP14) POI ovaries in POI mice. **D** Representative images of ovarian sections co-stained for PDGFD and PDGFRβ, along with quantification of fluorescence intensity in four groups of POI ovaries. **E** Representative images of IHC-stained ovarian sections and quantification with pPKC, pERK1/2 and MMP1 in three groups of control aging-, h-hADSCs-treated (h-hADSCs)-, and h-hADSCs/HEP14-treated (h-hADSCs/HEP14) aging ovaries in aging mice. **F** Representative images of ovarian sections co-stained for PDGFD and PDGFRβ, along with quantification of fluorescence intensity in three groups of aging ovaries. **G** The level of secreted MMP-1 in the various conditioned media, including c-hADSCs-CM (CTL), h-hADSCs-CM (HEP14), h-hADSCs+PKCi-CM (HEP14+Bis I) and h-hADSCs +ERKi-CM (HEP14+PD98059) by ELISA assay. **H**, **I** Tube formation of HUVECs and quantification with various conditioned media described above, assessed by tube-formation assay, with confirmation by IF staining for CD31 and quantification of the tube length and numbers of branching points. Data are presented as means ± SEM ($n = 3$). P values were calculated by one-way ANOVA, followed by Tukey-Kramer post hoc test. Changes were considered statistically significant when $P < 0.05$. Scale bar = 100 μm.

there was no statistically significant difference in pregnancy rates between treatments with collagen/ADSCs (7/9) and ADSCs (8/11), indicating that addition of ADSCs on soluble collagen scaffolds did not improve pregnant rate. Collectively, our findings highlight the superior efficacy of the h-hADSCs/HEP14 combination therapy in restoring fertility in POI mice and underscore its potential as an innovative treatment option for ovarian insufficiency. This approach stands out in the context of existing literature, offering a promising direction for further research and clinical application in the management of POI.

In summary, HEP14 markedly enhances the survival, anti-fibrotic, and proangiogenic capabilities of h-hADSCs, as well as their transdifferentiation into functional ovarian cells. Activation of the PKC-ERK1/2-MMP1, -PDGFD, and -STC1 signaling pathways by HEP14 is identified as the key mechanism underlying these effects. Both standalone h-hADSCs therapy and the combined therapy using h-hADSCs with HEP14/PLGA microspheres effectively promote ovarian regeneration and restore ovarian function in mouse models of POI and ARNA-OI. Notably, the combined therapy outperforms h-hADSCs alone, showing superior therapeutic outcomes. This new strategy holds significant potential for clinical application, pending further rigorous studies to confirm its safety and efficacy.

Materials and methods

Animal

Female (5~6 week-old and 12 month-old) and male (8~10-week old) C57BL/6N mice were purchased from the GemPharmatech. Co., Ltd (Jiangshu, China) and housed in the specific pathogen-free (SPF) environment with temperature control (22 ± 1 °C) and humidity control (60 ± 10%) on a 12 h light/12 h dark cycle with ad libitum access to water and regular rodent chow. We have complied with all relevant ethical regulations for animal use. All experimental procedures were approved by the Shenzhen Perking University-Hong Kong University of Science and Technology Medical Center of China Animal Care and Use Committee (Protocol number: 2023-147) and were conducted in accordance with the National Laboratory Animal Care and Use research committee guidelines.

Chemicals

HEP14 (5β-O-angelate-20-deoxyingenol), derived from Euphorbia peplus Linn plants by Professor Xiaojiang Hao's group[11], was dissolved in DMSO at 25 mM. Doxorubicin (Sigma) was prepared in DMSO at 50 mg/ml. Both the PKC inhibitor bisindolylmaleimide I (Bis1, Selleck) and the ERK inhibitor PD98059 (Selleck) were dissolved in DMSO at 10 mM.

Cell culture and collection of conditioned media

hADSCs were provided by co-author Professor Lin Bai from the Institute of Laboratory Animal Science, Chinese Academy of Medical Sciences. These cells were collected from healthy donors undergoing liposuction surgery. Prior to tissue collection, informed written consent was obtained from each donor. The study protocol and the use of hADSCs were approved by the Institutional Animal Care and Use Committee of the Institute of Laboratory Animal Science (Beijing, China) (License number: BL18004) and the Medical Ethics Committee of Plastic Surgery Hospital (Beijing, China) (License number: (2019)1-121). The investigators strictly adhered to the Declaration of Helsinki throughout the study. All ethical regulations relevant to human research participants were followed. hADSCs were isolated using the previously described method[21] with modifications and cultured in DMEM/F-12 medium supplemented with 10% FBS, 1% Glumax, 1% NEAA, and 1% penicillin/streptomycin at 37 °C in a 5% CO_2 incubator. Passage 4 hADSCs were used for experiments. Their morphology was observed by inverted microscopy. Osteogenic and adipogenic differentiation was assessed using inductive media and stained with Alizarin Red and Oil Red O, respectively. Conditioned media (CM) were collected from passage 4 hADSCs untreated (CTL-CM) or treated with HEP14 (HEP14-CM), HEP14+Bis (HEP14/PKCi-CM), or HEP14+PD98059 (HEP14/PG98057-CM). HUVECs were cultured in 199 media, and endothelial cell medium was used as a positive control (HUVECs-CM). All media were stored at −80 °C, and cells were imaged using light microscopy.

Flow cytometry assays

Human adipose-derived stem cells (hADSCs) were harvested and incubated with the following antibodies for 30 min at 4 °C: HLA-APC-Cy7 (clone LN3), CD34-PE-Cy7 (clone WM59), CD90-FITC (clone eBio5E10), CD73-PE (clone AD2), CD29-PerCP (clone MAR4), and CD105-APC (clone SN6). Flow cytometry data were collected using a FACS Aria II instrument (BD Biosciences, USA). The gating strategy was established based on the negative control and the forward scatter (FSC) and side scatter (SSC) profiles of hADSCs. Data analysis was performed using FlowJo software (BD Biosciences). All antibodies used are listed in Supplementary Table S2, unless noted otherwise.

Cell viability assay

The cell viability was assessed by a CCK-8 assay according to the manufacturer's instruction. Briefly, 6×10^3 cells per well were seeded into 96-well plates. After culturing overnight, the cells were treated with different concentrations of HEP4 for the indicated time. Then, 10 μL CCK-8 regent (MCE) was added to each well and incubated for 4 h at 37 °C. The absorbance was subsequently measured at 490 nm using a Microplate reader (Bio-Rad).

Calculation of population doubling time

hADSCs were digested with Tryple (Gibco) and the same number cells (1.5×10^4) were plated in each well of 24-well plate for subsequent evaluations. After 24, 48, 72 h of HEP14 treatment, hADSCs from two wells combined into a single tube before centrifugation to minimize cell loss and the number of cells were compared with the number of cells that were originally plated. Doubling time, or the time required for one cycle of cell division, was calculated using the following formula: Population Doubling time (h) = Cell culture time (h) /log2 (Collected cell number Plated cell number/ Plated cell number).

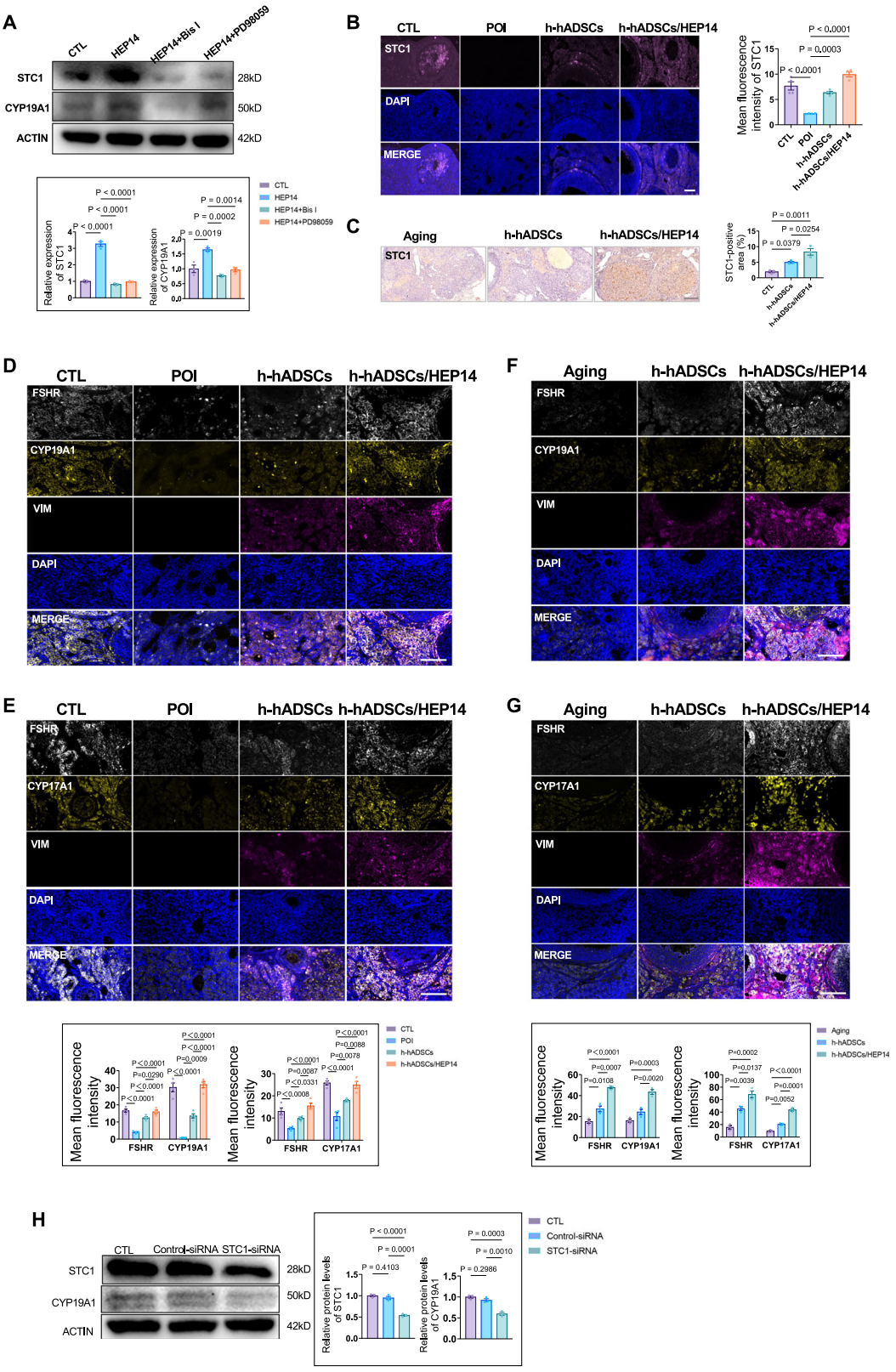

RNA-Seq and functional enrichment analysis

The treated hADSCs treated with either HEP14 (h-hADSCs) or DMSO (c-hADSCs) were collected after three PBS washes, and total RNA was extracted using TRIzol reagent. RNA sequencing libraries with 370–420 bp inserts were sequenced on the Illumina NovaSeq 6000 platform. Clean data was mapped to the reference genome using HISAT2, and gene expression levels were quantified using featureCounts. FPKM values were calculated for each gene. Differential expression analysis was performed using DESeq2, with a threshold of |log2 fold change|> 1 and adj. $p < 0.05$. GO and KEGG analysis of differentially expressed genes was conducted using clusterProfiler, and GSEA was performed with gsea v3.0.

Fig. 7 | h-hADSCs promote ovarian regeneration and functional recovery via HEP14-activated PKC-ERK1/2-STC1-CYP19A1 pathway. A Western blot analysis of protein expression and quantification of STC1 and CYP19A1 in h-hADSCs co-treated with either PKC inhibitor Blis1 or ERK1/2 inhibitor PD98059, compared to c-hADSCs. **B** Representative images of ovarian sections stained for STC1 by IF staining and quantification in four groups: normal control (CTL), vehicle-treated (POI)-, h-hADSCs-treated (h-hADSCs)-, and h-hADSCs/HEP14-treated (h-hADSCs/HEP14) POI ovaries in POI mice. **C** Representative images of ovarian sections stained for STC1 by IHC staining and quantification in three groups: control aging-, h-hADSCs-treated(h-hADSCs)-, and h-hADSCs/HEP14-treated (h-hADSCs/HEP14) aging ovaries in mice with ARNA-OI. **D** Representative images of ovarian sections stained for vimentin, FSHR, and Cyp19A1 by triple IF staining and quantification in four groups of POI ovaries. **E** Representative images of ovarian sections stained for vimentin, FSHR, and Cyp17A1 by triple IF staining and quantification in four groups of POI ovaries. **F** Representative images of ovarian sections stained for vimentin, FSHR, and Cyp19A1 by triple IF staining and quantification in three groups of aging ovaries. **G** Representative images of ovarian sections stained for vimentin, FSHR, and Cyp17A1 by triple IF staining and quantification in three groups of aging ovaries. **H** Protein expression and quantification of STC1 and CYP19A1 in KNG cells upon STC1 knockdown using STC1-specific siRNA, analyzed by Western blot. Data are presented as means ± SEM. $n = 4$ for (**D** to **E**), $n = 3$ for (**A** to **C**) and (**F** to **H**). P values were calculated by one-way ANOVA, followed by Tukey-Kramer post hoc test. Changes were considered statistically significant when $P < 0.05$. Scale bar = 100 μm.

Single-cell RNA sequencing (scRNA-seq)

h-hADSCs and c-hADSCs were digested into single-cell suspensions and processed using 10X Genomics Chromium microfluidic chips with 30 v2 chemistry. Up to 15,000 cells were used to generate scRNA-seq libraries, which were sequenced on the Illumina NovaSeq. Raw reads were demultiplexed and mapped to the reference genome using the 10X Genomics Cell Ranger pipeline. Downstream single-cell analyses were performed using Cell Ranger and Seurat[52,53]. Digital expression matrices were constructed by counting unique molecule identifiers for each gene and cell barcode. Secondary filtration was applied using Seurat, retaining genes expressed in >3 cells and cells with ≥200 expressed genes, while removing foreign cells. CellRanger reanalyze was used for dimensionality reduction, clustering, and gene expression analysis. The Seurat package was used for data normalization, and the CCA method[54] was used for integrated analysis of datasets.

RNA extraction, reverse transcription, and quantitative real-time polymerase chain reaction

Treated cells were harvested, and total RNA was extracted using TRIzol™ Reagent. cDNA was synthesized using the PrimeScript RT reagent Kit with gDNA Eraser. mRNA expression was quantified by SYBR Green Real-Time PCR using specific primers, with RPL19 as an endogenous control. Primer sequences are provided in Supplementary Data Table S1.

Western blots

Cells were lysed in ice-cold RIPA buffer containing protease and phosphatase inhibitors. Lysates were cleared by centrifugation, and protein concentrations were measured using a BCA kit. Proteins were denatured at 98 °C, and 20 μg per sample was resolved by 12% SDS-PAGE. Proteins were transferred to PVDF membranes, blocked, and incubated with the indicated antibodies, followed by detection with HRP-conjugated secondary antibodies. Blot signals were quantified using ImageJ. All antibodies used are listed in Supplementary Table S2, unless noted otherwise.

Trace of HEP14 residual in the supernatants containing h-hADSCs

hADSCs were divided into c-hADSCs and h-hADSCs groups. After 36-h incubation, the cells were washed with saline to remove residual HEP14, then resuspended and centrifuged in 0.5 mL of saline and centrifuged to pellet the cells. The resulting supernatants were extracted with ethyl acetate to quantify residual HEP14. The extracts were evaporated, and the residues resuspended in methanol for LC/MS analysis using the AB SCIEX Triple Quad 5500 system. A HEP14 standard in DMSO served as a positive control, and saline as a negative control. Data were acquired and processed using Analyst TF1.6 and PeakView software, with mass errors calculated and tolerated at <0.05 ppm.

Establishment of POI model mice

To establish a Doxorubicin-induced POI mouse model, 6~7-week-old female C57BL/6N mice were weighed, divided into two groups randomly ($n = 18$ each) and then treated with a single intraperitoneal injections of different doses (8 mg/kg, 12 mg/kg and 16 mg/kg) of Doxorucibin (Sigma) ($n = 18$/group) or an equal volume of saline solution as the control. At 1, 2, 4 weeks after treatment, mice were sacrificed using cervical dislocation for sample collection. Body weight, ovarian size, estrous cyclicity, serum hormone levels and follicle count and morphology were examined to evaluate the POI model.

Treatment of POI model mice, sample collection and fertility evaluation

To track the transplanted h-hADSCs in vivo, the cells were pre-labeled with 5 μM of CellTracker™ CM-DiI for 30 min (h-hADSCs$^{CM\text{-}DiI}$; Molecular probes, USA) and observed under fluorescent microscope (Leica). As indicated in the designed experimental procedures (Fig. 3A), 7~8 week-old female C57BL/6N mice were used as normal control (CTL mice, $n = 22$). The POI mice were further divided into three groups ($n = 22$ or 26 each). Both normal mice and POI mice were treated with saline by i.p. injection and by intraovarian (i.o.) injection, h-hADSCs mice were treated with h-hADSCs in saline by i.o. injection and saline by i.p. injection (the h-hADSCs therapy), and h-hADSCs/HEP14 mice were treated with h-hADSCs in saline by i.o. injection and HEP14/PLGA microspheres in saline at a dosage of 10 mg per kg of body weight by i.p. injection (the combined therapy). To minimize procedure time and variability, i.o. injections were performed only on the right ovary. At 2 weeks and 4 weeks following treatments, the samples ($n = 6$ or 8 each) were collected to evaluate changes of ovarian structure and function. At 4 weeks following treatments, the remaining mice ($n = 10$/group) were mated with fertile male (2:1) over a period of 2 weeks. Vaginal copulation plugs were checked in the morning for 2 weeks. Cesarean section was used to remove the fetus at gestation of 18 to 19 days. Fertility was assessed based on the total number of fetuses of each group and the average number of litters per mouse.

Treatment of aging mice, sample collection and fertility evaluation

12-month old female mice were divided into three groups ($n = 8$): control aging mice were treated with saline by i.p. injection and by intraovarian (i.o.) injection; h-hADSCs aging mice were treated with pre-labled h-hADSCs in saline by i.o. injection and saline by i.p. injection (the h-hADSCs therapy), and h-hADSCs/HEP14 aging mice were treated with pro-labeled hADSCs in saline by i.o. injection and HEP14/PLGA microspheres in saline at a dosage of 10 mg per kg of body weight by i.p. injection every 5 days for 30 consecutive days (the combined therapy). At 4 weeks following treatments, the samples were collected to evaluate changes of ovarian structure and function. Vaginal copulation plugs were checked in the morning for 2 weeks.

Estrous cyclicity

Vaginal smears were performed at 9:00 am every morning consecutively for 2 weeks to examine the estrous cycle before and after treatment. First, cotton swabs were moistened with saline, rotated gently in the vagina, and then smeared on adhesive slides. Next, the detached cells were observed in microscope to determine the different stages of the estrous cycle, such as proestrus, estrus, metoestrus and diestrus.

Hematoxylin-Eosin staining of ovarian sections, morphological analysis and follicle counts

Ovaries collected at specified time points were fixed in 4% paraformaldehyde for 24 h, then embedded in paraffin. To ensure the consistency and comparability of ovarian follicle counts across various experimental groups, we applied uniform follicle counting standards and correction factors to all analyzed samples, drawing on established methodologies[55–57]. This protocol utilizes systematic sampling, where six-micrometer sections were cut, beginning from one end of the ovarian tissue. Follicle counting began from the fifth section and was performed in every fifth section, with a total of eight consecutive sections being counted. Only those follicles in which the nucleus of the oocyte is clearly visible were included in the count. Subsequently, the total number of follicles counted in these eight sections was multiplied by 5 to estimate the total follicle count per ovary. Images were captured using an Aperio GT 450 microscope (Leica), and morphological characteristics of the ovarian sections were analyzed, with different follicle stages (primordial, primary, secondary, antral, atretic) and corpus luteum counted.

hADSCs were cultured on glass coverslips for 48 h, then washed, fixed with 4% paraformaldehyde, and permeabilized with 0.25% TritonX-100. Non-specific sites were blocked with 2% BSA in TBST. Slides were incubated with the NANOG primary antibody overnight at 4 °C, followed by washing and incubation with the goat anti-rabbit IgG (FITC) secondary antibody and DAPI for nuclei staining. Cells were observed under fluorescent microscopy (Leica).

TUNEL assay

Ovarian granulosa cell apoptosis was examined using a TUNEL assay kit (Servicebio) following the manufacturer's instructions, as previously described[58]. Briefly, deparaffinized tissue sections were incubated with proteinase K (20 mg/ mL) at 37 °C for 20 min, followed by incubation with permeabilization buffer at room temperature for 20 min. After equilibration at room temperature for 10 min, sections were incubated with terminal deoxynucleotidyl transferase and deoxyuridine triphosphate at 37 °C for 2 h in a moist chamber. Nuclei were counterstained with DAPI. Images were acquired using a Nikon Eclipse Ti-SR microscope.

Immunohistochemistry

Paraffin-fixed ovarian sections were incubated with primary mouse antibodies, including ER, FSHR, AMH, α-SMA, MMP1, p-PKCα, and p-ERK at 4 °C overnight. The slides were then incubated with the biotinylated secondary antibody including HRP labeled Goat anti-Rabbit IgG, HRP labeled Goat anti-mouse IgG at 37 °C for 30 min and developed with diaminobenzidine (DAB, Servicebio) as chromogen and then counterstained with hematoxylin. Images were acquired using the Pannoramic MIDI scanner (3DHISTECH). The IHC Profiler in ImageJ software (NIH) was used to analyze staining results. The average grayscale value (staining intensity) and percentage of positive area (staining area) of positive cells as IHC measurement indicators, four scores were ultimately given as High positive, Positive, Low positive, and Negative. All the antibodies used in this study were listed in the Supplementary Data Table S2, unless otherwise stated.

Multiple immunofluorescence labeling staining

Ovarian sections were incubated with primary mouse antibodies overnight at 4 °C, followed by incubation with corresponding secondary antibodies at 37 °C for 1 h. Nuclei were stained with DAPI, and images were captured using a Pannoramic MIDI scanner. Fluorophores FITC, SPRed, CY5, and DAPI emitted green, pink, pink, and blue light, respectively, at specified excitation and emission wavelengths. All antibodies used are listed in Supplementary Data Table S2.

Picrosirius red and Masson's trichrome staining for fibrosis analysis

Fibrosis in ovarian tissue was analyzed using Picrosirius Red (PSR) staining and Masson's Trichrome staining. Ovarian paraffin sections were deparaffinized by immersing twice in xylene for 5 min each, followed by sequential hydration in 90%, 70%, and 50% ethanol for 5 min each and twice in water for 5 min each. The sections were then stained with hematoxylin for 10 min to visualize nuclei, followed by PSR staining for 1 h to highlight collagen fibers. After a quick wash with acetic acid and absolute ethanol, the slides were rinsed with xylene and mounted with DPX mounting resin. To further determine the collagen volume fraction (CVF), Masson's trichrome staining was performed on the tissue sections using Masson's trichrome staining reagent (Solarbio, G1346, China) according to the manufacturer's instructions. The sections were stained with hematoxylin for 10 min to stain nuclei blue-black, followed by Masson's Trichrome staining to visualize collagen fibers (stained blue) and muscle/cytoplasm (stained red). Images of the stained sections were captured using an Aperio GT 450 microscope (Leica). The fibrotic areas in the PSR-stained ovarian sections were quantified using ImageJ software (NIH). Polarized light scanning was used to distinguish collagen type I (red) from type III fibrils (green) under a Nikon Eclipse ci polarized microscope. The CVF was calculated as the ratio of the blue-stained collagen area to the total ovarian section area, excluding the follicular cavity and vasculature.

Enzyme-linked immunosorbent assay (ELISA)

Blood samples were collected and serum was obtained by centrifuging at 5000 rpm for 10 min. The levels of serum anti-Müllerian hormone (AMH), estradiol (E2), Follicle-stimulating hormone (FSH), and the activity of MMP 1 were measured using the ELISA assays following the manufacturer's instructions. The ELISA kits for E2, AMH and FSH were purchased from Meimian industrial Co., Ltd (Jiangsu, China). The Functional sensitivity was 0.1 pg/mL for E2, 11.75 pg/mL for Amh and 0.1 mIU/mL for FSH. MMP1 were measured by ELISA Kit (FY-EH6011, Wuhan Feiyue Biotechnology Co., Ltd). Functional sensitivity was 0.128 ng/mL. The absorbance was subsequently measured at 450 nm using a microplate reader (Rayto). The concentration of these hormones was calculated based on the standard curve.

Tube formation assay

Matrigel matrix growth factor reduced (BD) was thawed, dispensed in 24-well plates, and solidified at 37 °C. HUVECs were seeded at a density of 5×10^4 cells, and incubated at 37 °C for 1 h. Cell culture inserts (0.8 μm pore; BD) was placed in each well. HUVECs were resuspended in various conditioned media 18 h. The network-like structures of HUVECs were examined under a microscope.CD31 expression was detected by IF staining. Angiogenic activities were quantified by measuring tube length using ImageJ.

Knockdown using siRNA

RNA oligonucleotides used for siRNA in this study are 5′-AUUUGAAUGUAAAGGACUCTT-3′, 5′-AGUAACAAAUUCAUGGCACTT-3′ and 5′-AUUUCAUACAACAGGACGCTT-3′. Cells were transfected with 100pmol RNA oligonucleotides twice in 6-well plates using Lipofectamine 3000. The knockdown effect of siRNA was evaluated 24 h after transfection by western blot.

Statistics and reproducibility

Data were expressed as the mean ± standard error of the mean (SEM) and analyzed using the GraphPad Prism 8.0 statistic software (GraphPad Software). Student's *t* test is used to compare the means between two groups. One-way ANOVA was used for the homogeneous variance in three or more group comparisons followed by the Tukey between groups. The sample sizes "*n*" refer to biologically independent samples/experiments, and the exact "*n*" values are indicated in the figure legends. A p value of <0.05 was considered to be a significant difference.

Reporting summary

Further information on research design is available in the Nature Portfolio Reporting Summary linked to this article.

Data availability

RNA-sequencing data in this manuscript are available at NCBI GEO under the accession numbers GSE273949 and GSE273950. Uncropped blot images are provided in Supplementary information as Fig. S6. Source data are provided in Supplementary Data 2 and 3. All data needed to evaluate the conclusions in the paper are present in the paper and/or the Supplementary Materials. Any additional data related to this study can be requested from the corresponding authors upon reasonable request.

Received: 26 January 2025; Accepted: 1 August 2025;
Published online: 23 August 2025

References

1. te Velde, E. R. & Pearson, P. L. The variability of female reproductive ageing. *Hum. Reprod. Update* **8**, 141–154 (2002).
2. Winkler, I. et al. The cycling and aging mouse female reproductive tract at single-cell resolution. *Cell* **187**, 981–998.e925 (2024).
3. Chon, S. J., Umair, Z. & Yoon, M. S. Premature ovarian insufficiency: past, present, and future. *Front. Cell Dev. Biol.* **9**, 672890 (2021).
4. Wesevich, V., Kellen, A. N. & Pal, L. Recent advances in understanding primary ovarian insufficiency. *F1000Res* **9**, https://doi.org/10.12688/f1000research.26423.1 (2020).
5. Wilkosz, P., Greggains, G. D., Tanbo, T. G. & Fedorcsak, P. Female reproductive decline is determined by remaining ovarian reserve and age. *PLoS ONE* **9**, e108343 (2014).
6. Sullivan, S. D., Sarrel, P. M. & Nelson, L. M. Hormone replacement therapy in young women with primary ovarian insufficiency and early menopause. *Fertil. Steril.* **106**, 1588–1599 (2016).
7. Galipeau, J. & Sensébé, L. Mesenchymal stromal cells: clinical challenges and therapeutic opportunities. *Cell Stem Cell* **22**, 824–833 (2018).
8. Qin, Y. et al. An update on adipose-derived stem cells for regenerative medicine: where challenge meets opportunity. *Adv. Sci.***10**, e2207334 (2023).
9. Silva, L. H., Cruz, F. F., Morales, M. M., Weiss, D. J. & Rocco, P. R. Magnetic targeting as a strategy to enhance therapeutic effects of mesenchymal stromal cells. *Stem Cell Res. Ther.* **8**, 58 (2017).
10. Li, Q. et al. Drug-free in vitro activation combined with ADSCs-derived exosomes restores ovarian function of rats with premature ovarian insufficiency. *J. Ovarian Res.* **17**, 158 (2024).
11. Li, Y. et al. Protein kinase C controls lysosome biogenesis independently of mTORC1. *Nat. Cell Biol.* **18**, 1065–1077 (2016).
12. Nishizuka, Y. Intracellular signaling by hydrolysis of phospholipids and activation of protein kinase C. *Science* **258**, 607–614 (1992).
13. Su, J. et al. Transplantation of adipose-derived stem cells combined with collagen scaffolds restores ovarian function in a rat model of premature ovarian insufficiency. *Hum. Reprod.* **31**, 1075–1086 (2016).
14. Jones, A. S. K. et al. Cellular atlas of the human ovary using morphologically guided spatial transcriptomics and single-cell sequencing. *Sci. Adv.* **10**, eadm7506 (2024).
15. Castrillon, D. H., Miao, L., Kollipara, R., Horner, J. W. & DePinho, R. A. Suppression of ovarian follicle activation in mice by the transcription factor Foxo3a. *Science* **301**, 215–218 (2003).
16. Wan, B., Bao, Q. & Burgess, D. Long-acting PLGA microspheres: advances in excipient and product analysis toward improved product understanding. *Adv. Drug Deliv. Rev.* **198**, 114857 (2023).
17. Harguindey, A. et al. Synthesis and assembly of click-nucleic-acid-containing PEG-PLGA nanoparticles for DNA delivery. *Adv. Mater.* **29**, https://doi.org/10.1002/adma.201700743 (2017).
18. Gui, L. et al. HEP14 treatment improves ovarian function in aged mice through mitophagy enhancement and oxidative stress reduction. *Commun. Biol.* **8**, 1141 (2025).
19. Harrell, C. R. et al. Molecular mechanisms responsible for therapeutic potential of mesenchymal stem cell-derived secretome. *Cells* **8**, https://doi.org/10.3390/cells8050467 (2019).
20. Zhao, Y. X. et al. Using mesenchymal stem cells to treat female infertility: an update on female reproductive diseases. *Stem Cells Int.* **2019**, 9071720 (2019).
21. Zuk, P. A. et al. Human adipose tissue is a source of multipotent stem cells. *Mol. Biol. Cell* **13**, 4279–4295 (2002).
22. Dutta, S. & Sengupta, P. Men and mice: relating their ages. *Life Sci.* **152**, 244–248 (2016).
23. Hinz, B. et al. The myofibroblast: one function, multiple origins. *Am. J. Pathol.* **170**, 1807–1816 (2007).
24. Zimmermann, R. C. et al. Vascular endothelial growth factor receptor 2-mediated angiogenesis is essential for gonadotropin-dependent follicle development. *J. Clin. Invest.* **112**, 659–669 (2003).
25. Kakuta, H., Iguchi, T. & Sato, T. The involvement of granulosa cells in the regulation by gonadotropins of Cyp17a1 in theca cells. *Vivo* **32**, 1387–1401 (2018).
26. Hatzirodos, N., Hummitzsch, K., Irving-Rodgers, H. F. & Rodgers, R. J. Transcriptome comparisons identify new cell markers for theca interna and granulosa cells from small and large antral ovarian follicles. *PLoS ONE* **10**, e0119800 (2015).
27. Nishi, Y. et al. Establishment and characterization of a steroidogenic human granulosa-like tumor cell line, KGN, that expresses functional follicle-stimulating hormone receptor. *Endocrinology* **142**, 437–445 (2001).
28. Karnezis, A. N. et al. Re-assigning the histologic identities of COV434 and TOV-112D ovarian cancer cell lines. *Gynecol. Oncol.* **160**, 568–578 (2021).
29. Giaccari, C., Antonouli, S., Anifandis, G., Cecconi, S. & Di Nisio, V. An update on physiopathological roles of Akt in the ReprodAKTive mammalian ovary. *Life* **14**, https://doi.org/10.3390/life14060722 (2024).
30. Nguyen, V. H. L., Hough, R., Bernaudo, S. & Peng, C. Wnt/β-catenin signalling in ovarian cancer: Insights into its hyperactivation and function in tumorigenesis. *J. Ovarian Res.* **12**, 122 (2019).
31. Wörthmüller, J. & Rüegg, C. The crosstalk between FAK and Wnt signaling pathways in cancer and its therapeutic implication. *Int. J. Mol. Sci.* **21**, https://doi.org/10.3390/ijms21239107 (2020).
32. Mohamed, S. A. et al. Human mesenchymal stem cells partially reverse infertility in chemotherapy-induced ovarian failure. *Reprod. Sci.* **25**, 51–63 (2018).
33. Wang, S. et al. Single-cell transcriptomic atlas of primate ovarian aging. *Cell* **180**, 585–600.e519 (2020).
34. Jin, C. et al. The regulatory landscapes of human ovarian ageing. Preprint at *bioRxiv* https://www.biorxiv.org/content/10.1101/2022.05.18.492547v1 (2022).
35. Nguyen, H. H., Milat, F. & Vincent, A. Premature ovarian insufficiency in general practice: meeting the needs of women. *Aust. Fam. Physician* **46**, 360–366 (2017).
36. Kawano, T., Inokuchi, J., Eto, M., Murata, M. & Kang, J. H. Activators and inhibitors of protein kinase C (PKC): their applications in clinical trials. *Pharmaceutics* **13**, https://doi.org/10.3390/pharmaceutics13111748 (2021).
37. Nagase, H., Visse, R. & Murphy, G. Structure and function of matrix metalloproteinases and TIMPs. *Cardiovasc. Res.* **69**, 562–573 (2006).
38. Vincenti, M. P. & Brinckerhoff, C. E. Transcriptional regulation of collagenase (MMP-1, MMP-13) genes in arthritis: integration of complex signaling pathways for the recruitment of gene-specific transcription factors. *Arthritis Res.* **4**, 157–164 (2002).
39. Hwu, Y. M. et al. Luteinizing hormone increases platelet-derived growth factor-D gene expression in human granulosa-luteal cells. *Fertil. Steril.* **92**, 2065–2068 (2009).
40. Chang, A. C., Dunham, M. A., Jeffrey, K. J. & Reddel, R. R. Molecular cloning and characterization of mouse stanniocalcin cDNA. *Mol. Cell Endocrinol.* **124**, 185–187 (1996).

41. Varghese, R., Wong, C. K., Deol, H., Wagner, G. F. & DiMattia, G. E. Comparative analysis of mammalian stanniocalcin genes. *Endocrinology* **139**, 4714–4725 (1998).
42. Shen, L., Liu, J., Luo, A. & Wang, S. The stromal microenvironment and ovarian aging: mechanisms and therapeutic opportunities. *J. Ovarian Res.* **16**, 237 (2023).
43. Umehara, T. et al. Female reproductive life span is extended by targeted removal of fibrotic collagen from the mouse ovary. *Sci. Adv.* **8**, eabn4564 (2022).
44. Yoshiko, Y. et al. Evidence for stanniocalcin gene expression in mammalian bone. *Endocrinology* **140**, 1869–1874 (1999).
45. Guzmán, A., Hughes, C. H. K. & Murphy, B. D. Orphan nuclear receptors in angiogenesis and follicular development. *Reproduction* **162**, R35–r54 (2021).
46. Luo, C. W., Kawamura, K., Klein, C. & Hsueh, A. J. Paracrine regulation of ovarian granulosa cell differentiation by stanniocalcin (STC) 1: mediation through specific STC1 receptors. *Mol. Endocrinol.* **18**, 2085–2096 (2004).
47. Wang, H., Eriksson, H. & Sahlin, L. Estrogen receptors alpha and beta in the female reproductive tract of the rat during the estrous cycle. *Biol. Reprod.* **63**, 1331–1340 (2000).
48. Levy, O. et al. Shattering barriers toward clinically meaningful MSC therapies. *Sci. Adv.* **6**, eaba6884 (2020).
49. Hoang, D. M. et al. Stem cell-based therapy for human diseases. *Signal Transduct. Target Ther.* **7**, 272 (2022).
50. Shojafar, E., Soleimani Mehranjani, M. & Shariatzadeh, S. M. A. Adipose derived mesenchymal stem cells improve the structure and function of autografted mice ovaries through reducing oxidative stress and inflammation: a stereological and biochemical analysis. *Tissue Cell* **56**, 23–30 (2019).
51. Bahrehbar, K. et al. Human embryonic stem cell-derived mesenchymal stem cells improved premature ovarian failure. *World J. Stem Cells* **12**, 857–878 (2020).
52. Satija, R., Farrell, J. A., Gennert, D., Schier, A. F. & Regev, A. Spatial reconstruction of single-cell gene expression data. *Nat. Biotechnol.* **33**, 495–502 (2015).
53. Macosko, E. Z. et al. Highly parallel genome-wide expression profiling of individual cells using nanoliter droplets. *Cell* **161**, 1202–1214 (2015).
54. Butler, A., Hoffman, P., Smibert, P., Papalexi, E. & Satija, R. Integrating single-cell transcriptomic data across different conditions, technologies, and species. *Nat. Biotechnol.* **36**, 411–420 (2018).
55. Bucci, T. J., Bolon, B., Warbritton, A. R., Chen, J. J. & Heindel, J. J. Influence of sampling on the reproducibility of ovarian follicle counts in mouse toxicity studies. *Reprod. Toxicol.* **11**, 689–696 (1997).
56. Tilly, J. L. Ovarian follicle counts-not as simple as 1, 2, 3. *Reprod. Biol. Endocrinol.* **1**, 11 (2003).
57. Myers, M., Britt, K. L., Wreford, N. G., Ebling, F. J. & Kerr, J. B. Methods for quantifying follicular numbers within the mouse ovary. *Reproduction* **127**, 569–580 (2004).
58. Lv, S. J., Hou, S. H., Gan, L. & Sun, J. Establishment and mechanism study of a primary ovarian insufficiency mouse model using lipopolysaccharide. *Anal. Cell Pathol.* **2021**, 1781532 (2021).

Acknowledgements

We extend our gratitude to all co-authors for their invaluable contributions to this manuscript. These studies were supported by: Sanming Project of Medicine in Shenzhen (No. SZSM202011016). Shenzhen High-level Hospital Construction Fund (YBH2019-260). National Natural Science Foundation of China (U1812403 to Dr Liming Gui). National Natural Science Foundation of China (82293683 to Prof Xiaojiang Hao).

Author contributions

Conceptualization: L.G. Methodology: L.G., J.S., Q.Z., K.L., Q.S., L.B., Y.D. B.T. and X.H. Investigation: L.G., J.S., Q.Z., K.L., Q.S., L.B., Y.D., B.T., and C.L. Visualization: L.G., J.S., and Q.Z. Supervision: L.G., B.T., X.H. Writing original draft: L.G. Writing editing and review: L.G., J.S., Q.Z., H.P., B.T., and X.H.

Competing interests

The authors declare no competing interests.

Additional information

Supplementary information The online version contains supplementary material available at https://doi.org/10.1038/s42003-025-08656-x.

Correspondence and requests for materials should be addressed to . Tang, Xiaojiang Hao or Liming Gui.

Peer review information *Communications Biology* thanks the anonymous reviewers for their contribution to the peer review of this work. Primary Handling Editors: Eirini Trompouki and Johannes Stortz. [A peer review file is available].